Electronic Supplementary Material (ESI) for Chemical Communications.

Supporting information

An Earth-abundant System for Light-driven CO_2 Reduction to CO Using a Pyridinophane Iron Catalyst

Yuto Sakaguchi,[a] Arnau Call,*[b] Mihaela Cibian,[a] Kosei Yamauchi,[a,b] Ken Sakai*[a,b,c]

[a] *International Institute for Carbon-Neutral Energy Research (WPI-I2CNER), Kysuhu University, Motooka, 744, Nishi-ku, Fukuoka 819-0395, Japan.*
[b] *Department of Chemistry, Faculty of Science, Kyushu University, Motooka, 744, Nishi-ku, Fukuoka 819-0395, Japan.*
[c] *Center of Molecular Systems (CMS), Kyushu University, Motooka, 744, Nishi-ku, Fukuoka, 918-0395, Japan.*

*Corresponding authors email address:

arnau_call@chem.kyushu-univ.jp

ksakai@chem.kyushu-univ.jp

Table of Contents

1. Materials and reagents. All solvents were of the highest quality available and were used as received. Photosensitizer [Cu(bathocuproine)(xantphos)]PF_6 (**Cu-PS**) was synthesized according to literature procedures.[1] All other reagents were purchased from Tokyo Chemical Industry Co., and used without further purification. Purification of water (0.055 µS) was performed with a RFD250RB water distillation apparatus.

2. Instrumentation. UV-Visible absorption spectra were recorded on a Shimadzu UV-2600 and a Shimadzu UV-2600 spectrophotometer, respectively. Emission decays were recorded on a HORIBA FluoroCube 3000USKU. The excitation source was a diode laser (λ=379 nm) (HORIBA N-470L). All the sample solutions were maintained at 25 ºC during the spectrophotometric measurements. ESI-TOF-MS spectra were recorded on a JEOL JMS-T100LC mass spectrometer in positive or negative ion mode. FT-IR spectra were acquired on a PerkinElmer Spectrum One FT-IR Spectrometer. ^{1}H NMR spectra were acquired on a JEOL JNM-ESA 600 and JNM-ECS 400 spectrometers. Cyclic voltammetry experiments were recorded on a BAS ALS Model 602DKM electrochemical analyzer using a three electrode system consisting of a glassy carbon working electrode, a platinum wire counter electrode, and a Ag/Ag^+ reference electrode (0.249 V vs. SCE), where Bu_4NPF_6 (tetra-*n*-butylammonium hexafluorophosphate) was used as a supporting electrolyte. All reported potentials are given relative to Fc/Fc^+ couple (Fc/Fc^+ = 0.450 vs. SCE). The quantification of gases was done using Shimadzu GC-14A equipped with a molecular sieve 13X-S Å column of 2 m x 3 mm *i.d.*, at 30 ºC. The injection of the sample gas (200 µL) was performed manually using a gas-tight syringe and the output signal from the thermal conductivity detector of the gas chromatograph was analyzed using a Shimadzu C-R8A integrator. The CO and H_2 peaks were determined using calibration curves which had been previously obtained using standard CO and H_2 gas. Photoirradiation experiments were carried out by an ILC Technology CERMAX LX-300 Xe lamp (179 $mW \cdot cm^{-2}$, 220 A, 300 V) equipped with a CM-1 cold mirror which reflects lights in the range of $400 < \lambda < 800$ nm. The photolysis vial (21 mL) was immersed in a 25 ºC water bath to remove IR radiation and to eliminate the temperature effects. The ^{13}CO generated during irradiation was detected by GC-MS (HP 6890 Series GC SYSTEM, 5973 Mass Selective Detector).

3. X-ray diffraction measurements and structure determination. Crystallographic data for the solid state structures presented and discussed herein were collected at 100 K, from single crystals mounted on a fiber loop. Data were collected using a Bruker SMART APEX II Charged-Coupled Device (CCD) Area Detector diffractometer. The crystal-to-detector distance was 6.0 cm. The X-ray source was a monochromated Mo-Kα radiation (λ = 0.71073 Å) from a rotating anode with a mirror focusing apparatus operated at 1.2 kW (50 kV, 24 mA). For data collection, determination of cell parameters, cell refinement, and data reduction, *APEX2* and *SAINT* (Bruker, 2009 and Bruker, 2013) were used.[2] Absorption corrections were applied using *SADABS* (Bruker 2014).[3] Employing *OLEX2*(Dolomanov *et al.*, 2009),[4] the structure solutions were performed using *SHELXT* Intrinsic Phasing (Sheldrick, 2008; Sheldrick, 2015)[5] and refined on F^2 by full-matrix least squares using *SHELXL2014* (Sheldrick, 2008; Sheldrick, 2015).[5] *OLEX2* (Dolomanov *et al.*, 2009),[4] *ORTEP-3 for Windows* (Farrugia, 2012),[6] Mercury,[7] and POV-ray (2013)[8] were used for molecular graphics. The material was prepared for publication using *PLATON* (Spek, 2009),[9] Mercury,[7] and *publCIF* (Westrip, 2010).[10]

4. Photocatalytic experiments and chromatographic detection of gases. In a typical photocatalytic run, a 5 mL DMF:TEOA (4:1 *v/v*) mixed solution containing catalyst (0.05 mM in metal), **Cu-PS** (0.5 mM) and BIH (50 mM) was purged with CO_2 (purity ≥ 99.995 %) for 15 min prior to irradiation. The temperature was held constant at 25 ºC throughout the experiment. The gases generated from the reaction during the photolysis were quantified by GC-TCD measurements of 200 µL aliquots from the reaction vial headspace.

5. Earth-abundant photocatalytic systems reported in the literature

Beller et al. (2017)[11a]

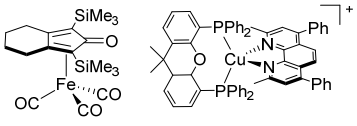

Cat: Fe-Cat **PS: Cu-PS**

TON_{CO} = 487, Sel_{CO2} = 99%

Ishitani et al. (2016)[11b]

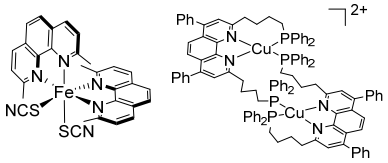

Cat: $[Fe(qpy)(OH_2)_2]^{2+}$ **PS: Cu-PS_d**

TON_{CO} = 273, Sel_{CO2} = 78%

Lau et al. (2016)[11c]

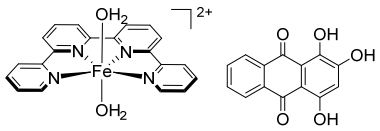

Cat: $[Fe(qpy)(OH_2)_2]^{2+}$ **PS: Purpurin**

TON_{CO} = 1365, Sel_{CO2} = 92%

Bian et al. (2016)[11d]

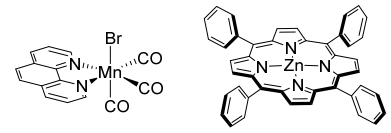

Cat: *fac*-Mn(phen)$(CO)_3$Br **PS: ZnTPP**

TON_{CO} = 119, Sel_{CO2} = 86%

Robert et al. (2017)[11e]

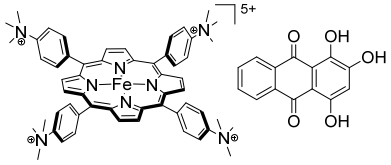

Cat: Fe-*p*-TMA **PS: Purpurin**

TON_{CO} = 120, Sel_{CO2} = 95%

Robert et al. (2017)[11f]

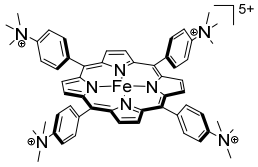

Cat: Fe-*p*-TMA

TON_{CO} = 101, Sel_{CO2} = 100%

Ishitani et al. (2018)[11g]

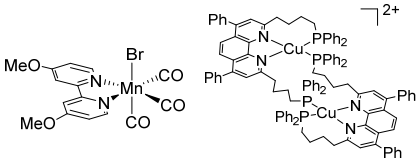

Cat: *fac*-Mn(4,4'-OMe -bpy)$(CO)_3$Br **PS: Cu-PS_d**

TON_{CO} = 1004, Sel_{CO2} = 97%

Beller et al. (2019)[11h]

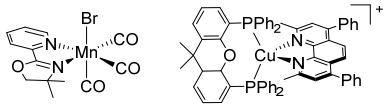

Cat: *fac*-[Mn(pyrox)$(CO)_3$Br **PS: Cu-PS**

TON_{CO} = 1058, Sel_{CO2} = 99%

Lau et al. (2019)[11i]

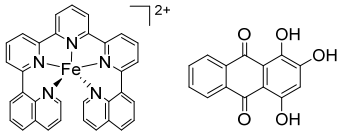

Cat: $[Fe(dptpy)]^{2+}$ **PS: Purpurin**

TON_{CO} = 544, Sel_{CO2} = 99%

Robert et al. (2018)[11j]

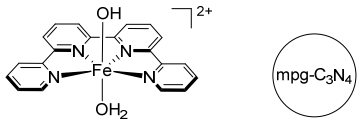

Cat: $[Fe(qpy)(OH_2)_2]^{2+}$ **PS: mpg-C_3N_4**

TON_{CO} = 155, Sel_{CO2} = 97%

He et al. (2018)[11k]

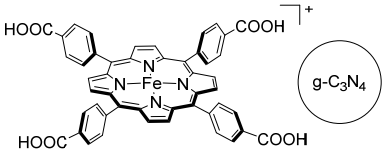

Cat: FeTCPP **PS: g-C_3N_4**

TON_{CO} = 5.7, Sel_{CO2} = 100%

Reisner et al. (2018)[11l]

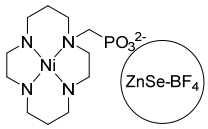

Cat: NiCycP **PS: ZnSe-BF_4**

TON_{CO} = 283, Sel_{CO2} = 34%

Reisner et al. (2017)[11m]

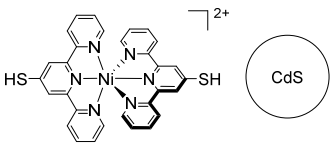

Cat: $[Ni(terpyS)_2]^{2+}$ **PS: CdS**

TON_{CO} = ~20, Sel_{CO2} = 92%

Lu et al. (2018)[11n]

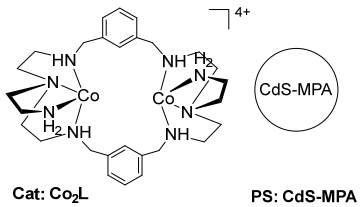

Cat: Co_2L **PS: CdS-MPA**

TON_{CO} = 1380, Sel_{CO2} = 95%

Fig. S1. Photocatalytic systems for CO_2-to-CO reduction based on earth-abundant elements.[11]

6. Synthesis of metal complexes

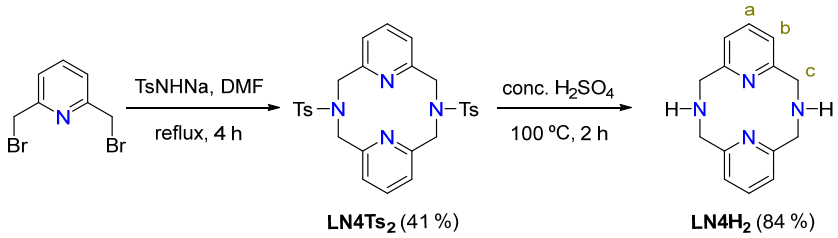

Scheme S1. Synthesis of the **LN4H$_2$** ligand.

Synthesis of 2,11-diaza[3,3](2,6)pyridinophane (LN4H$_2$). **LN4H$_2$** ligand was synthesized following reported method slightly modificatied[12] To a solution of TsNHNa (0.965 g, 5 mmol) in 100 mL dry DMF at 80 °C, a solution of 2,6-bis(bromomethyl)pyridine (1.32 g, 5 mmol) in 10 mL dry DMF was added dropwise under Ar atmosphere. After stirring for 1 h, TsNHNa (0.965 g, 5 mmol) was added all at once. The reaction mixture was stirred at 80 °C for 4 h and cooled to room temperature. The solution was concentrated by rotary evaporation, and the white precipitate was filtered. The resulting white solid was purified by silica gel column chromatography (eluent CH_2Cl_2 with an increasing amount of AcOEt) to give **LN4Ts$_2$** (0.566 g, 1.03 mmol, 41% yield). After that, the tosylated **LN4Ts$_2$** ligand (0.400 g, 0.73 mmol) was dissolved in conc. H_2SO_4 (3.7 mL) and refluxed for 2 h. After cooling to room temperature, the solution was basified with NaOH, and the resulting mixture was extracted with $CHCl_3$ (3 x 50 mL). The combined organic layers were dried over anhydrous Na_2SO_4 and the solvent was removed under reduced pressure to give the **LN4H$_2$** ligand as a colourless powder (0.148 g, 0.62 mmol, 84% yield). ^{1}H NMR ($CDCl_3$, 600 MHz, 293 K): δ = 7.09 (t, *J* = 7.6 Hz, 2H, **H$_a$**) 6.51 (d, *J* = 7.6 Hz, 4H, **H$_b$**) 3.94 (s, 8H, **H$_c$**).

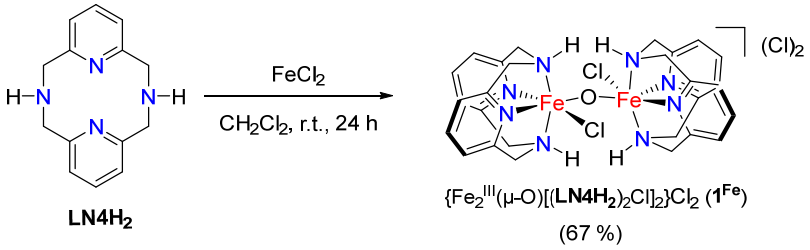

Scheme S2. Synthesis of the **{[Fe^{III}(LN4H$_2$)Cl]$_2$(μ-O)}Cl$_2$** (**1^{Fe}**) complex.

Synthesis of {[Fe^{III}(LN4H$_2$)Cl]$_2$(μ-O)}Cl$_2$. At ambient temperature, a solution of **LN4H$_2$** ligand (0.100 g, 0.42 mmol) in 3 mL CH_2Cl_2 was added to a stirred suspension of $FeCl_2$ (0.053 g, 0.42 mmol) in 2 mL CH_2Cl_2. The resulting pale yellow solution gradually became cloudy and a brown precipitate appeared. After stirring for an additional 8 hours, the solution was filtered off and the resulting solid was dried under vacuum. The obtained solid was dissolved in CH_3OH (2 mL), filtered through Celite© and crystallized by slow diffusion of ether into CH_3OH yielding 0.103 g of a brown crystalline solid (0.28 mmol, 67 % yield). ^{1}H NMR (CD_3OD, 600 MHz, 293 K): δ = 114.16, 97.43, 36.34, 31.88, 17.46, 13.64, 7.50, 7.17. ESI-TOF MS (m/z): 284.06 $[C_{14}H_{14}N_4Fe]^+$. Elemental analysis calculated for $C_{28}H_{32}Cl_4N_8Fe_2O+H_2O$: C, 43.78; H, 4.46; N, 14.59%. Found: C, 43.77; H, 4.42; N, 14.52%.

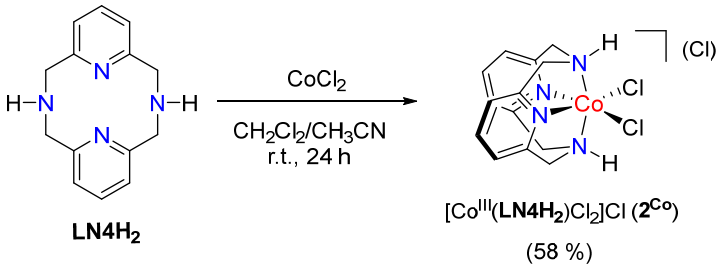

Scheme S3. Synthesis of the **[Co^{III}(LN4H$_2$)Cl$_2$]Cl** (**2^{Co}**) complex.

Synthesis of [Co^{III}(LN4H$_2$)Cl$_2$]Cl. At ambient temperature, a solution of **LN4H$_2$** ligand (0.100 g, 0.42 mmol) in 3 mL CH_2Cl_2 was added to a stirred suspension of $CoCl_2$ (0.054 g, 0.42 mmol) in 2 mL CH_2Cl_2. After stirring for an additional 8 hours, the solution was filtered off and the resulting purple precipitate dried under vacuum. The obtained solid was dissolved in CH_3OH (2 mL), filtered through Celite© and crystallized by slow diffusion of ether into CH_3OH yielding 0.089 g of a purple crystalline solid (0.24 mmol, 58 % yield). ^{1}H NMR (CD_3OD, 600 MHz, 293 K): δ = 8.02, 7.54, 4.48, 4.12. ESI-TOF MS (m/z): 334.04 $[C_{14}H_{16}N_4ClCo]^+$. Elemental analysis calculated for $C_{14}H_{16}Cl_3N_4Co+1.5H_2O$: C, 38.84; H, 4.89; N, 12.94%. Found: C, 39.03; H, 4.64; N, 12.76%.

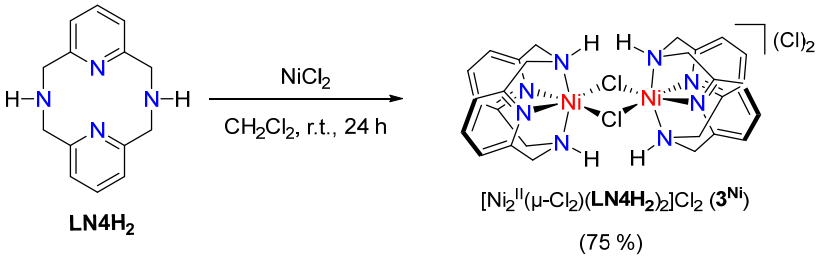

Scheme S4. Synthesis of the **[Ni^{II}(LN4H$_2$)(μ-Cl)]$_2$Cl$_2$** (**3^{Ni}**) complex.

Synthesis of [Ni^{II}(LN4H$_2$)(μ-Cl)]$_2$Cl$_2$. At ambient temperature, a solution of **LN4H$_2$** ligand (0.060 g, 0.25 mmol) in 3 mL CH_2Cl_2 was added to a stirred mixture of $NiCl_2{\cdot}6H_2O$ (0.059 g, 0.25 mmol) in 10 mL CH_2Cl_2:CH_3CN (1:1). After stirring for an additional 3 days, the pale purple precipitate was filtered and dried under vacuum. The obtained solid was dissolved in H_2O (1 mL) and crystallized by slow diffusion of acetone into H_2O yielding 0.073 g of a pale purple crystalline solid (0.19 mmol, 75 % yield). ^{1}H NMR (CD_3OD, 600 MHz, 293 K): δ = 111.08, 59.93, 12.85. ESI-TOF MS (m/z) 333.04 $[C_{14}H_{16}N_4ClNi]^+$. Elemental analysis calculated for $C_{14}H_{16}Cl_2N_4Ni+H_2O$: C, 43.35; H, 4.68; N, 14.44%. Found: C, 43.29; H, 4.56; N, 14.49%.

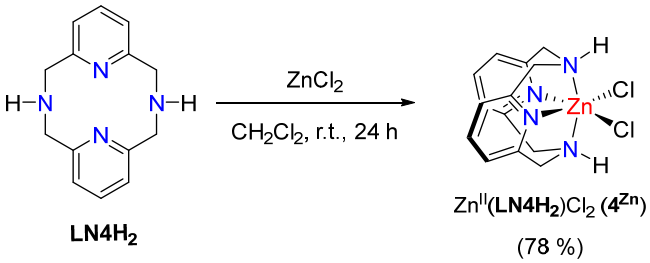

Scheme S5. Synthesis of the $\mathbf{Zn^{II}(LN4H_2)Cl_2}$ ($\mathbf{4^{Zn}}$) complex.

Synthesis of $\mathbf{Zn^{II}(LN4H_2)Cl_2}$. At ambient temperature, a solution of **$LN4H_2$** ligand (0.056 g, 0.23 mmol) in 5 mL CH_2Cl_2 was added to a stirred suspension of $ZnCl_2$ (0.032 g, 0.23 mmol) in 5 mL CH_2Cl_2. After stirring for an additional 24 hours the solution was filtered off and the resulting colourless precipitate dried under vacuum. The obtained solid was dissolved in CH_3OH (2 mL), filtered through Celite© and crystallized by slow diffusion of ether into CH_3OH yielding 0.068 g of a colourless crystalline solid (0.18 mmol, 78 % yield). ^{1}H NMR ($CDCl_3$, 600 MHz, 293 K): δ = 7.67 (t, *J* = 7.7 Hz, 2H, $\mathbf{H_a}$) 7.15 (d, *J* = 7.7 Hz, 4H, $\mathbf{H_b}$) 5.15 (t, *J* = 6.9 Hz, 2H, $\mathbf{H_d}$) 4.56 (dd, *J* = 6.9 and 16.5 Hz, 4H, $\mathbf{H_c}$) 3.92 (d, *J* = 16.5 Hz, 4H, $\mathbf{H_c}$). ESI-TOF MS (m/z): 338.94 $[C_{14}H_{16}N_4ClZn]^+$. Elemental analysis calculated for $C_{14}H_{16}Cl_2N_4Zn+1.5H_2O$: C, 41.66; H, 4.75; N, 13.88%. Found: C, 41.26; H, 4.58; N, 13.53%.

7. Characterization of metal complexes

XRD crystallography

Crystal data and structure refinement details for compounds $\mathbf{1^{Fe}}$, $\mathbf{2^{Co}}$, $\mathbf{3^{Ni}}$ and $\mathbf{4^{Zn}}$ are summarized in Table S1. Selected bond lengths and angles are presented in Tables S2-S5, whereas Tables S6-S10 show comparisons of structural parameters with those in reported relevant complexes. The hydrogen bonding geometries for $\mathbf{1^{Fe}}$, $\mathbf{2^{Co}}$, $\mathbf{3^{Ni}}$ and $\mathbf{4^{Zn}}$ are highlighted in Table S11. The solid state structures of $\mathbf{1^{Fe}}$, $\mathbf{2^{Co}}$, $\mathbf{3^{Ni}}$ and $\mathbf{4^{Zn}}$ are presented in Fig. S2-S5. The corresponding H-bonding patterns and packing interactions are illustrated in Fig. S6-S13. For all the structures presented herein, unless otherwise stated, all non-H atoms were refined by full-matrix least-squares with anisotropic displacement parameters. The H-atoms were included in calculated positions and treated as riding atoms: aromatic C—H 0.95 Å, methyl C—H 0.98 Å, with $U_{iso}(H) = k \times U_{eq}$ (parent C-atom), where k = 1.2 for the aromatic H-atoms and 1.5 for the methyl H-atoms. The H-atoms connected to heteroatoms (N atoms) were in all cases located from the difference Fourier map and they were freely refined.

Crystallographic data for $\mathbf{1^{Fe}}$, $\mathbf{2^{Co}}$, $\mathbf{3^{Ni}}$ and $\mathbf{4^{Zn}}$ were deposited in CCDC.[13] The corresponding CCDC numbers are given in Table S1. Validation of the crystallographic information files (cifs) with the checkCIF/ PLATON routine was performed, returning only C and G level alerts. The comments to these alerts are included in the cifs of the corresponding compounds.

Compound $\mathbf{1^{Fe}}$ ({Fe^{III}[(**LN4H$_2$**)Cl]$_2$(μ-O)}Cl_2•solvent)

The structure of compound $\mathbf{1^{Fe}}$ was obtained from the best available crystal, which unfortunately was poor quality, resulting in mediocre overall quality of the data set. SQUEEZE routine (*PLATON* (Spek, 2009),[9]) as implemented in *OLEX2* (Dolomanov *et al.*, 2009)[4] was used to remove co-crystallized disordered solvent molecules present in the structure. As a result, an improvement of the R_1 factor with ~ 9.6 % was obtained. The presence of three co-crystallized methanol molecules can be estimated based on the volumes of the accessible voids found (472 Å^3 per unit cell), the corresponding calculated number of electrons (108 electrons) (Z = 2), the insights obtained from the attempts to model the disordered solvent, and the identity of the solvents used for crystallization (methanol/ diethylether).

Compound $\mathbf{2^{Co}}$ ([Co^{III}(**LN4H$_2$**)Cl_2]Cl • solvent)

The solid state structure of $\mathbf{2^{Co}}$ contains co-crystallized disordered solvent molecules. As the attempts to model them were unsuccessful, they were removed using SQUEEZE routine (*PLATON* (Spek, 2009),[9]) as implemented in *OLEX2* (Dolomanov *et al.*, 2009).[4] As a result, an improvement of the R_1 factor with ~ 11.2 % was obtained. It can be estimated that one methanol molecule (or two water molecules) could fit. This estimation is based on calculated solvent accessible voids of 119 Å^3 per unit cell, containing 38 electrons (Z = 2), as well as on the insights obtained from the attempts to model the disordered solvent and the identity of the solvents used for crystallization (methanol/ diethylether).

Compound $\mathbf{3^{Ni}}$ ([Ni^{II}(**LN4H$_2$**)(μ-Cl)]$_2$$Cl_2$ • solvent)

The structure of compound $\mathbf{3^{Ni}}$ was obtained from the best available crystal, which unfortunately was poor quality, resulting in poor overall quality of the data set. SQUEEZE routine (*PLATON* (Spek, 2009),[9]) as implemented in *OLEX2* (Dolomanov *et al.*, 2009)[4] was used to remove co-crystallized disordered solvent molecules present in the structure. As a result, an improvement of the R_1 factor with ~ 5.7 % was obtained. The presence of 1.5 co-crystallized methanol molecules can be estimated based on calculated solvent accessible voids of 328 Å^3 per unit cell, containing 57 electrons (Z = 2), as well as on the insights obtained from the attempts to model the disordered solvent and the identity of the solvents used for crystallization (methanol/ diethylether).

Compound $\mathbf{4^{Zn}}$ (Zn^{II}(**LN4H$_2$**)Cl_2 • solvent)

The solid state structure of $\mathbf{4^{Zn}}$ contains co-crystallized disordered solvent molecules. They were removed using SQUEEZE routine (*PLATON* (Spek, 2009),[9]) as implemented in *OLEX2* (Dolomanov *et al.*, 2009).[4] As a result, an improvement of the R_1 factor with ~ 6.2 % was obtained. It can be estimated that one methanol molecule (or 1.5 water molecules) could fit. This estimation is based on calculated solvent accessible voids of 1600 Å^3 per unit cell, containing 260 electrons (Z = 16), as well as on the insights obtained from the attempts to model the disordered solvent and the identity of the solvents used for crystallization (methanol/ diethylether). The weight second parameter is unusually large for $\mathbf{4^{Zn}}$ (7.77), which can indicate twinning. No twin law was detected with TwinRotMat routine from *PLATON* (Spek, 2009).[9] However, twinning was identified upon inspection of the diffraction pattern in *RLATT* (Bruker, 2013).[2] Treatment for non-merohedrally twinned crystal data was performed using *CELL_NOW* (2 domains)/ *TWINABS*/ *BASF* / *HKLF5* (Bruker 2014)[3], but the models obtained were worse than the present model. Therefore the twinning treatment was not retained.

Table S1. Crystal data for $\mathbf{1^{Fe}}$, $\mathbf{2^{Co}}$, $\mathbf{3^{Ni}}$ and $\mathbf{4^{Zn}}$.

	$\mathbf{1^{Fe}}$	$\mathbf{2^{Co}}$	$\mathbf{3^{Ni}}$	$\mathbf{4^{Zn}}$
Compound	**$\{[Fe^{III}(LN4H_2)Cl]_2(\mu\text{-}O)\}Cl_2$ • solvent**	**$[Co^{III}(LN4H_2)Cl_2]Cl$ • solvent**	**$[Ni^{II}(LN4H_2)(\mu\text{-}Cl)]_2Cl_2$ • solvent**	**$Zn^{II}(LN4H_2)Cl_2$ • solvent**
CCDC no.	1892442	1892441	1892443	1892444
Empirical formula	$C_{28}H_{32}Cl_4Fe_2N_8O$	$C_{14}H_{16}Cl_3CoN_4$	$C_{28}H_{32}Cl_4N_8Ni_2$	$C_{14}H_{16}Cl_2N_4Zn$
Formula weight	750.11	405.59	739.83	376.58
Temperature/K	100	100	100	100
Crystal system	triclinic	triclinic	monoclinic	orthorhombic
Space group	P-1	P-1	C2/m	Fddd
a/Å	9.1131(16)	9.1082(10)	17.178(5)	8.6064(12)
b/Å	11.477(2)	9.8312(10)	8.837(3)	28.201(4)
c/Å	18.784(3)	9.9666(11)	12.505(4)	29.216(4)
α/°	98.812(2)	93.6550(10)	90	90
β/°	92.127(2)	98.8980(10)	112.309(3)	90
γ/°	91.893(2)	90.0060(10)	90	90
Volume/Å^3	1938.6(6)	879.88(16)	1756.3(9)	7090.8(17)
Z	2	2	2	16
ρ_{calc}g/cm^3	1.285	1.531	1.399	1.411
μ/mm^{-1}	1.055	1.431	1.406	1.685
F(000)	768.0	412.0	760.0	3072.0
Crystal size/mm^3	0.18 × 0.09 × 0.06	0.08 × 0.06 × 0.02	0.18 × 0.04 × 0.02	0.12 × 0.05 × 0.02
Radiation	MoKα (λ = 0.71073)	MoKα (λ = 0.71073)	MoKα (λ = 0.71073)	MoKα (λ = 0.71073)
2θ range for data collection/°	2.196 to 54.34	4.146 to 58.176	3.52 to 55.054	4.014 to 54.948
Index ranges	-11 ≤ h ≤ 11, -14 ≤ k ≤ 14, -24 ≤ l ≤ 24	-12 ≤ h ≤ 11, -13 ≤ k ≤ 13, -12 ≤ l ≤ 13	-22 ≤ h ≤ 22, -11 ≤ k ≤ 11, -16 ≤ l ≤ 16	-11 ≤ h ≤ 11, -36 ≤ k ≤ 36, -37 ≤ l ≤ 37
Reflections collected	22027	10731	10269	19628
Independent reflections	8518 [R_{int} = 0.0435, R_{sigma} = 0.0516]	4301 [R_{int} = 0.0243, R_{sigma} = 0.0298]	2150 [R_{int} = 0.0789, R_{sigma} = 0.0579]	2041 [R_{int} = 0.0453, R_{sigma} = 0.0238]
Data/restraints/parameters	8518/0/404	4301/0/207	2150/0/112	2041/0/100
Goodness-of-fit on F^2	1.058	1.066	1.040	1.070
Final R indexes [I>=2σ (I)]	R_1 = 0.0588, wR_2 = 0.1574	R_1 = 0.0332, wR_2 = 0.0925	R_1 = 0.0565, wR_2 = 0.1521	R_1 = 0.0299, wR_2 = 0.0784
Final R indexes [all data]	R_1 = 0.0715, wR_2 = 0.1645	R_1 = 0.0370, wR_2 = 0.0961	R_1 = 0.0777, wR_2 = 0.1644	R_1 = 0.0397, wR_2 = 0.0842
Largest diff. peak/hole / e Å^{-3}	0.93/-0.40	0.69/-0.55	1.46/-0.58	0.86/-0.30

[a] disordered co-crystallized solvent was removed using SQUEEZE routine (*PLATON* (Spek, 2009))[9] as implemented in *OLEX2 (Dolomanov et al., 2009)*.[4] (see text).

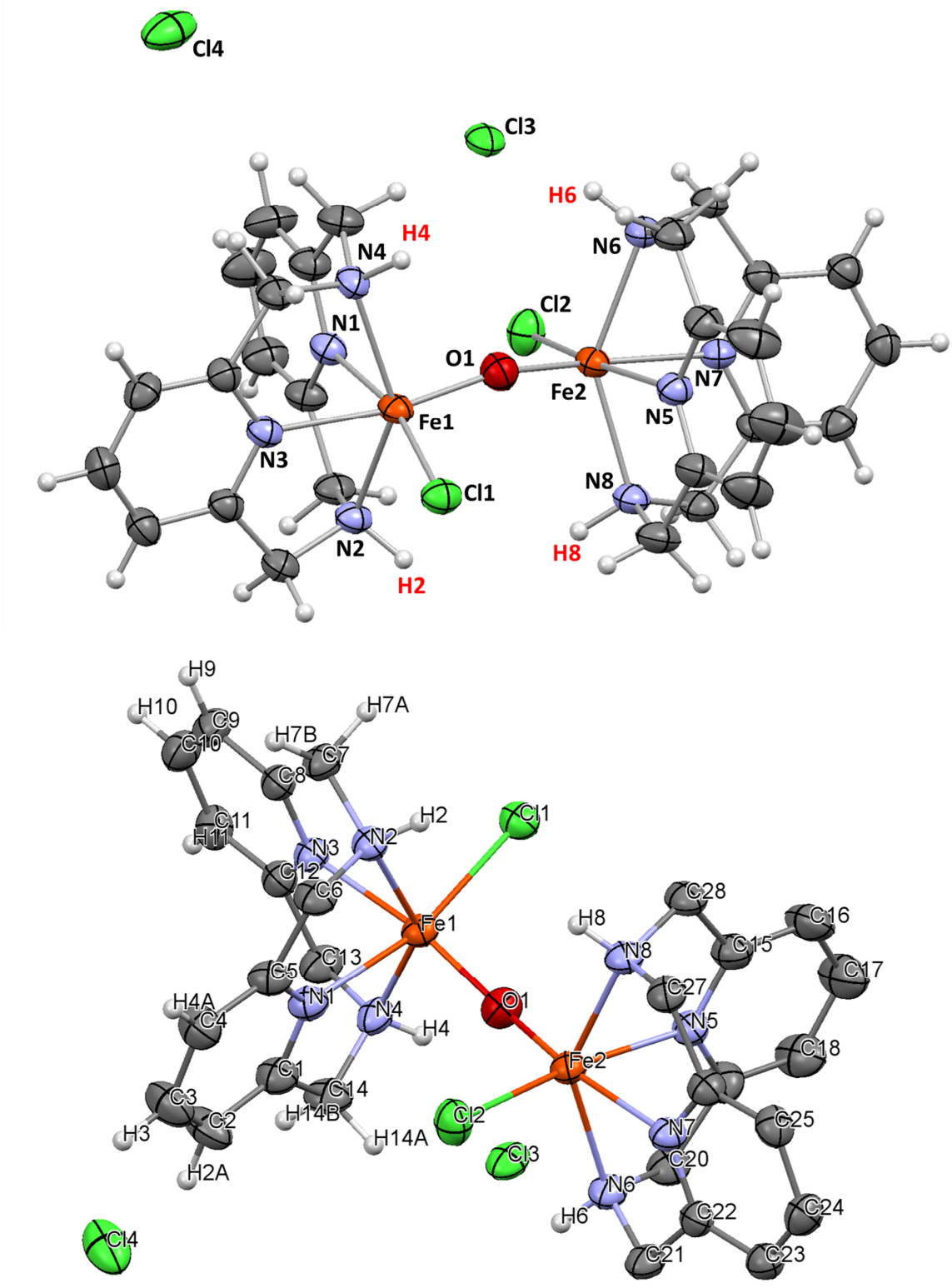

Fig. S2. The solid state structure of **1**^{Fe} (**{[Fe^{III}(LN4H$_2$)Cl]$_2$(μ-O)}Cl$_2$ • solvent**): best view (top); with labelled atoms (bottom). ORTEP view at 50% probability level.

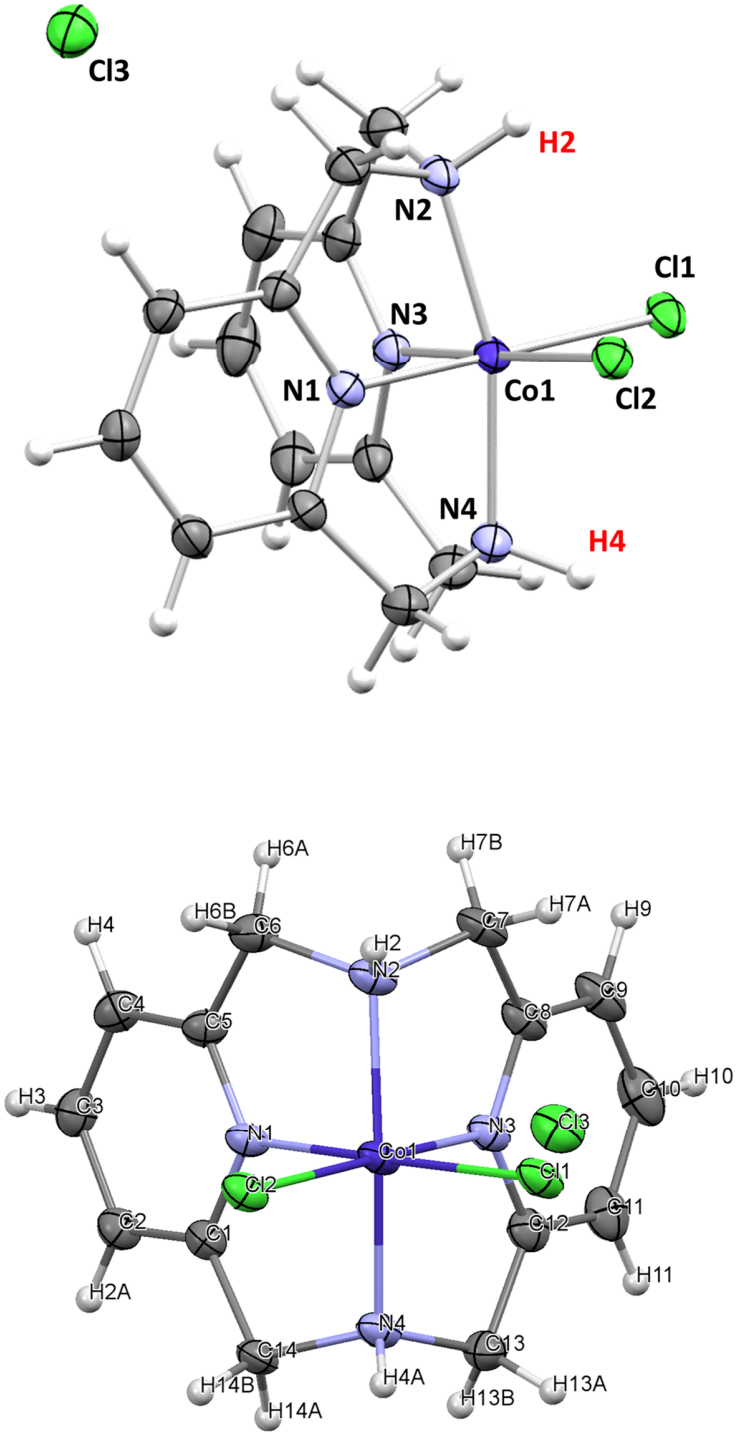

Fig. S3. The solid state structure of $\mathbf{2^{Co}}$ (**[Co^{III}(LN4H_2)Cl_2]Cl • solvent**): best view (top); with labelled atoms (bottom). ORTEP view at 50% probability level.

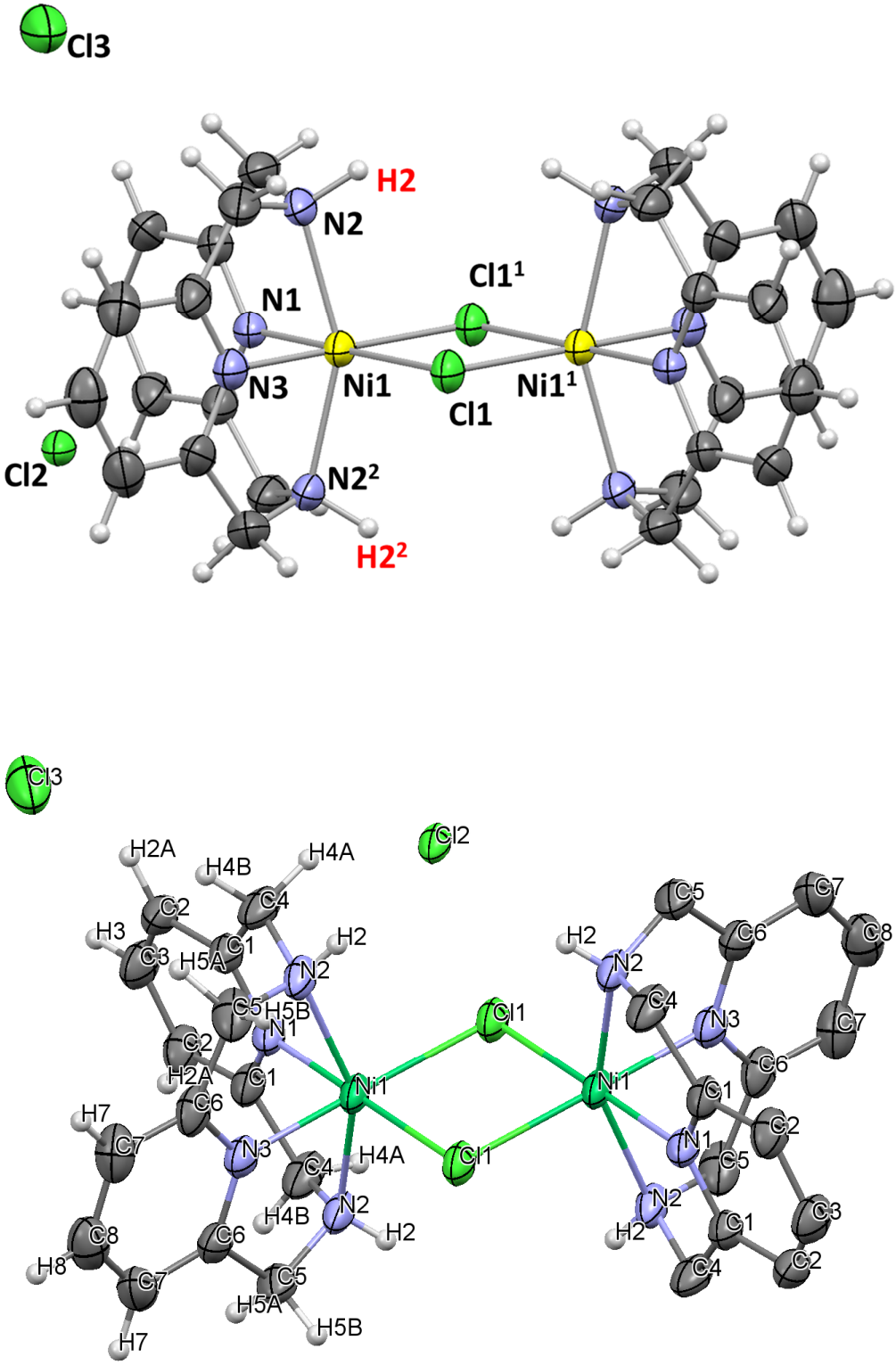

Fig. S4. The solid state structure of **3^{Ni} ([Ni^{II}(LN4H$_2$)(μ-Cl)]$_2$Cl$_2$ • solvent):** best view (top); with labelled atoms (bottom). ORTEP view at 50% probability level. Symmetry codes: [1]1-X, 1-Y, 1-Z; [2]+X, 1-Y, +Z.

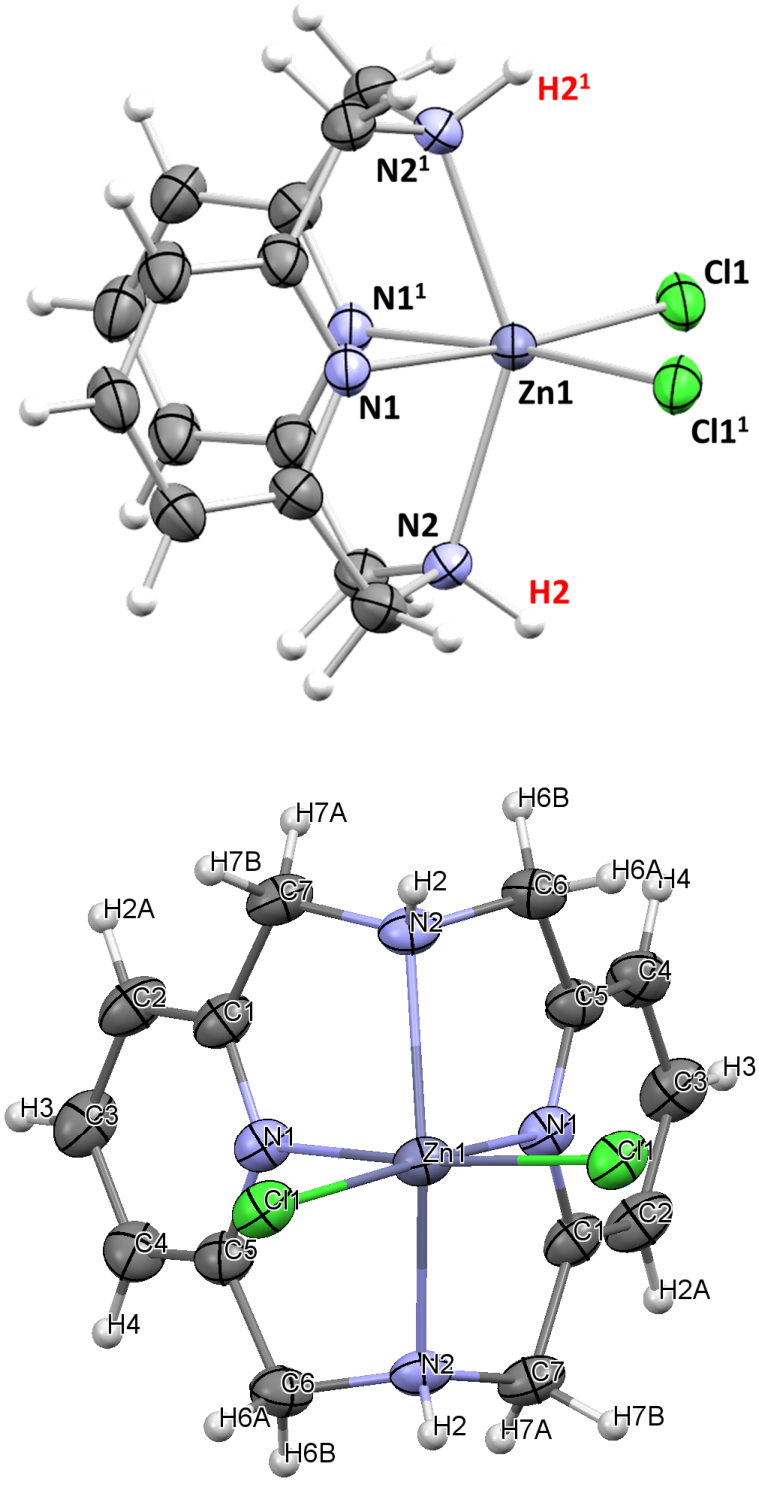

Fig. S5. The solid state structure of **4^{Zn}** (**Zn^{II}(LN4H$_2$)Cl$_2$ • solvent**): best view (top); with labelled atoms (bottom). ORTEP view at 50% probability level. Symmetry code: [1]7/4-X, 3/4-Y, +Z.

Table S2. Selected bond lengths (Å) and angles (°) for compound 1^{Fe} ({[Fe^{III}(**LN4H$_2$**)Cl]$_2$(μ-O)}Cl_2 • solvent)

Bond length (Å)/ angle (°)		Bond length (Å)/ angle (°)	
Fe1-Cl1	2.329(1)	Fe2-Cl2	2.301(1)
Fe1-O1	1.776(3)	Fe2-O1	1.775(3)
Fe1-N1	2.125(3)	Fe2-N5	2.134(3)
Fe1-N2	2.209(3)	Fe2-N6	2.224(3)
Fe1-N3	2.149(3)	Fe2-N7	2.152(3)
Fe1-N4	2.229(3)	Fe2-N8	2.212(3)
O1-Fe1-Cl1	98.9(1)	O1-Fe2-Cl2	98.9(1)
O1-Fe1-N1	93.4(1)	O1-Fe2-N5	90.8(1)
O1-Fe1-N2	109.5(1)	O1-Fe2-N6	101.6(1)
O1-Fe1-N3	170.6(1)	O1-Fe2-N7	170.8(1)
O1-Fe1-N4	96.0(1)	O1-Fe2-N8	102.8(1)
N1-Fe1-Cl1	166.4(1)	N5-Fe2-Cl2	170.3(1)
N1-Fe1-N2	75.8(1)	N5-Fe2-N6	76.3(1)
N1-Fe1-N3	81.1(1)	N5-Fe2-N7	80.0(1)
N1-Fe1-N4	76.5(1)	N5-Fe2-N8	75.8(1)
N2-Fe1-Cl1	94.5(1)	N6-Fe2-Cl2	101.9(1)
N2-Fe1-N4	143.1(1)	N7-Fe2-Cl2	90.3(1)
N3-Fe1-Cl1	87.5(1)	N7-Fe2-N6	75.6(1)
N3-Fe1-N2	76.7(1)	N7-Fe2-N8	75.8(1)
N3-Fe1-N4	75.4(1)	N8-Fe2-Cl2	101.5(1)
N4-Fe1-Cl1	107.8(1)	N8-Fe2-N6	142.9(1)
Fe2-O1-Fe1	158.6(1)		

Table S3. Selected bond lengths (Å) and angles (°) for compound **2^{Co}** ([Co^{III}(**LN4H$_2$**)Cl$_2$]Cl • solvent)

Bond length (Å)/ angle (°)		Bond length (Å)/ angle (°)	
Co1-Cl1	2.263(1)	Co1-Cl2	2.255(1)
Co1-N1	1.875(1)	Co1-N2	1.987(1)
Co1-N3	1.873(1)	Co1-N4	1.978(1)
N1-Co1-Cl1	178.5(1)	N3-Co1-N1	89.8(1)
N1-Co1-Cl2	90.0(1)	N3-Co1-Cl2	179.0(1)
N1-Co1-N2	83.8(1)	N3-Co1-N2	84.2(1)
N1-Co1-N4	84.1(1)	N3-Co1-N4	84.2(1)
Cl2-Co1-Cl1	91.5(1)	N4-Co1-Cl1	96.0(1)
N2-Co1-Cl1	95.8(1)	N4-Co1-Cl2	94.8(1)
N2-Co1-Cl2	96.8(1)	N4-Co1-N2	163.3(1)
N3-Co1-Cl1	88.8(1)		

Table S4. Selected bond lengths (Å) and angles (°) for compounds **3^{Ni}** ([Ni^{II}(**LN4H$_2$**)(μ-Cl)]$_2$Cl$_2$ • solvent)

Bond length (Å)/ angle (°)		Bond length (Å)/ angle (°)	
Ni1-Cl1	2.405(1)	Ni1-Cl1^1	2.414(1)
Ni1-N1	2.009(4)	Ni1-N2	2.155(3)
Ni1-N3	2.007(4)	Ni1-N2^2	2.155(3)
Cl1-Ni1-Cl1^1	87.5(1)	N2-Ni1-Cl1^1	99.9(1)
N1-Ni1-Cl1	179.4(1)	N2^2-Ni1-Cl1^1	99.9(1)
N1-Ni1-Cl1^1	91.9(1)	N2^2-Ni1-N2	152.9(1)
N1-Ni1-N2^2	80.5(9)	N3-Ni1-N1	89.0(1)
N1-Ni1-N2	80.5(9)	N3-Ni1-Cl1^1	179.1(1)
N2-Ni1-Cl1	99.6(1)	N3-Ni1-Cl1	91.6(1)
N2^2-Ni1-Cl1	99.6(1)	Ni1-Cl1-Ni1^1	92.5(1)
Symmetry codes: ^{1}1-X, 1-Y, 1-Z; ^{2}+X, 1-Y, +Z			

Table S5. Selected bond lengths (Å) and angles (°) for compound **4^{Zn}** (**$Zn^{II}(LN4H_2)Cl_2$ • solvent**)

Bond length (Å)/ angle (°)		Bond length (Å)/ angle (°)	
Zn1-Cl1	2.386(1)	Zn1-Cl1[1]	2.386(1)
Zn1-N1	2.128(1)	Zn1-N2	2.276(1)
Zn1-N1[1]	2.128(1)	Zn1-N2[1]	2.276(1)
Cl1-Zn1-Cl1[1]	93.5(1)	N1-Zn1-N2	76.3(1)
N1-Zn1-Cl1	172.7(1)	N1[1]-Zn1-N2[1]	76.3(1)
N1-Zn1-Cl1[1]	92.9(1)	N2[1]-Zn1-Cl1[1]	106.2(1)
N1[1]-Zn1-Cl1[1]	172.7(1)	N2-Zn1-Cl1[1]	98.2(1)
N1[1]-Zn1-Cl1	92.9(1)	N2-Zn1-Cl1	106.2(1)
N1-Zn1-N1[1]	81.0(1)	N2[1]-Zn1-Cl1	98.2(1)
N1[1]-Zn1-N2	76.7(1)	N2-Zn1-N2[1]	144.3(1)
N1-Zn1-N2[1]	76.7(1)		

Symmetry code: [1]7/4-X, 3/4-Y, +Z

Table S6. Comparison of averaged[a] bond distances (Å) and angles (º) in $\mathbf{1^{Fe}}$ with those in selected relevant dimeric complexes $\{[Fe^{III}(\mathbf{L})Cl]_2(\mu\text{-}O)\}X_2$ (**L** = tetradentate aminopyridiyl and tetraaza κ^4N type ligands)

Compound	$\mathbf{1^{Fe}}$ $\{[Fe^{III}(\mathbf{LN4H_2})Cl]_2(\mu\text{-}O)\}Cl_2 \bullet$ solvent	$\{[Fe^{III}(\mathbf{L1})Cl]_2(\mu\text{-}O)\}Cl_2 \bullet CH_3COCH_3 \bullet 2H_2O$	$\{[Fe^{III}(\mathbf{L2})Cl]_2(\mu\text{-}O)\}(I_3)_2$	$\{[Fe^{III}(\mathbf{L3})Cl]_2(\mu\text{-}O)(ClO_4)_2$	$\{[Fe^{III}(\mathbf{L4})Cl]_2(\mu\text{-}O)\}Cl_2 \bullet 2H_2O$
$Fe\text{-}N_{eq}$	$Fe\text{-}N_{eq} = Fe\text{-}N_{py}$ 2.130(2) (*trans* Cl) 2.151(3) (*trans* μ-O)	$Fe\text{-}N_{eq} = Fe\text{-}N_{amine}$ 2.188(4) (*trans* Cl) 2.328(4) (*trans* μ-O)	$Fe\text{-}N_{eq} = Fe\text{-}N_{amine}$ 2.200(7) (*trans* Cl) 2.237(7) (*trans* μ-O)	$Fe\text{-}N_{eq} = Fe\text{-}N_{amine}$ 2.202(6) (*trans* Cl) $Fe\text{-}N_{eq} = Fe\text{-}N_{py}$ 2.262(5) (*trans* μ-O)	$Fe\text{-}N_{eq} = Fe\text{-}N_{amine}$ 2.186(4) (*trans* Cl) 2.261(4) (*trans* μ-O)
$Fe\text{-}N_{axial}$	$Fe\text{-}N_{axial} = Fe\text{-}N_{amine}$ 2.219(2)	$Fe\text{-}N_{axial} = Fe\text{-}N_{py}$ 2.161(3)	$Fe\text{-}N_{axial} = Fe\text{-}N_{py}$ 2.188(5)	$Fe\text{-}N_{axial} = Fe\text{-}N_{py}$ 2.120(5)	$Fe\text{-}N_{axial} = Fe\text{-}N_{amine}$ 2.170(3)
Fe-Cl	2.301(1) – 2.329(1)	2.328(2)	2.339(3)	2.318(3)	2.352(1)
Fe-O	1.776(2)	1.806(1)	1.798(1)	1.790(1)	1.812(3)
$N_{eq}\text{-}Fe\text{-}N_{eq}$	$N_{py}\text{-}Fe\text{-}N_{py}$ 80.6(1)	$N_{amine}\text{-}Fe\text{-}N_{amine}$ 77.4(1)	$N_{amine}\text{-}Fe\text{-}N_{amine}$ 77.8(3)	76.8(2)	$N_{amine}\text{-}Fe\text{-}N_{amine}$ 77.7(1)
$N_{axial}\text{-}Fe\text{-}N_{axial}$	$N_{amine}\text{-}Fe\text{-}N_{amine}$ 143.0(1)	$N_{py}\text{-}Fe\text{-}N_{py}$ 166.9(2)	$N_{py}\text{-}Fe\text{-}N_{py}$ 160.3(2)	$N_{py}\text{-}Fe\text{-}N_{py}$ 154.6(1)	$N_{amine}\text{-}Fe\text{-}N_{amine}$ 147.6(1)
O-Fe-Cl	98.9(1)	104.5(1)	100.7(1)	101.2(1)	97.9(1)
Cl-Fe-Cl	-	-	-	-	-
Fe-O-Fe	158.6(1)	152.3(3)	180	180	178.9(3)
Fe···Fe	3.49(1)	3.51(1)	3.57(1)	3.58(1)	3.62(1)
CCDC ref./no.	1892442	RINNAD	PEWPUC	VIGHAP10	GUZLUI
Reference	this work	[14]	[15]	[16]	[17]

$\mathbf{LN4H_2}$ = 2,11-diaza[3,3](2,6)pyridinophane;

L1 = bispicMeen = *N,N'*-bis(2-pyridylmethyl)-*N'*-methylethane-1,2-diamine);

L2 = bispicen = *N,N'*-bis(2-pyridylmethyl)ethane-1,2-diamine;

L3 = TPA = tris(2-pyridylmethyl)amine;

L4 = 1,4,7,10-tetraazabicyclo[5.5.2]tetradecane

[a]values are averaged when they are identical within 3σ, otherwise the range of values is given; the error was calculated using the formula for propagation of error in calculations

Table S7. Comparison of averaged[a] bond distances (Å) and angles (º) in $\mathbf{1^{Fe}}$ with those in selected relevant monomeric complexes $[Fe(\mathbf{LN4R_2})X_2]^n$ ($\mathbf{N4R_2}$ = diazapyridinophane type ligands)

Compound	$\mathbf{1^{Fe}}$ {$[Fe^{III}(\mathbf{LN4H_2})Cl]_2(\mu\text{-}O)$} Cl_2 • solvent	$[Fe^{III}(\mathbf{LN4H_2})Cl_2]Cl$	$Fe^{II}(\mathbf{LN4Me_2})Cl_2$	$[Fe^{III}(\mathbf{LN4Me_2})Cl_2](ClO_4)$ • CH_3CN	$[Fe^{II}(\mathbf{LN4^tBu_2})Cl2]_3$ • $4H_2O$	$Fe^{II}(\mathbf{LN4^tBu_2})(OTf)_2$	$[Fe^{III}(\mathbf{LN4^tBu_2})(OMe)_2](OTf)$
Fe-N_{py}	2.130(2) (*rans* Cl) 2.151(3) (*trans* μ-O)	2.094(1)	2.177	2.129(1)	2.152(6)	2.093(1)	2.114(2) 2.134(2)
Fe-N_{amine}	2.219(2)	2.189(1)	2.298	2.229(1)	2.409(7) – 2.464(7)	2.354(1)	2.318(2) 2.352(2)
Fe-Cl	2.301(1) – 2.329(1)	2.289(5)	*n.r.*	2.241(1)	2.373(2) – 2.435(2)	-	-
Fe-O	1.776(2)	-	-	-	-	2.077(1)	1.865(1)
N_{py}-Fe-N_{py}	80.6(1)	85.0(1)	76	77.5(1)	79.9(3)	84.9(1)	81.0(1)
N_{amine}-Fe-N_{amine}	143.0(1)	142.4(1)	142.9	146.2(1)	137.5(3)	140.4(1)	140.1(1)
O-Fe-Cl	98.9(1)	-	-	-	-	90.2(1) (O-Fe-O)	99.0(1) (O-Fe-O)
Cl-Fe-Cl	-	94.7(1)	*n.r.*	99.8(1)	95.1(1) – 98.0(1)	-	-
CCDC ref./no.	1892442	RONXEX	*n.r.*	OPOVAR	ACISOU	HICRES	HICROC
Reference	this work	[18]	[19]	[20]	[21]	[22]	[22]

$\mathbf{LN4H_2}$ = 2,11-diaza[3,3](2,6)pyridinophane

$\mathbf{LN4Me_2}$ = *N,N'*-dimethyl-2,11-diaza[3,3](2,6)pyridinophane

$\mathbf{LN4^tBu_2}$ = *N,N'*-di-*tert*-butyl-2,11-diaza[3,3](2,6)pyridinophane

[a]values are averaged when they are identical within 3σ, otherwise the range of values is given; the error was calculated using the formula for propagation of error in calculations

n.r. = not reported

Table S8. Comparison of averaged[a] bond distances (Å) and angles (º) in **2^{Co}** with those in selected relevant monomeric complexes [Co(**LN4R$_2$**)X$_2$]^n (**LN4R$_2$** = diazapyridinophane type ligands)

Compound	**2^{Co}** [Co^{III}(**LN4H$_2$**)Cl$_2$]Cl • solvent	[Co^{II}(**LN4Me$_2$**)]Cl$_2$ • 2H$_2$O	[Co^{II}(**LN4^{t}Bu$_2$**)Cl$_2$]$_3$ • 4H$_2$O	Co^{II}(**LN4^{t}Bu$_2$**)Cl$_2$ • 0.5H$_2$O • CH$_3$OH
Co-N$_{py}$	1.874(1)	2.107(2)	2.091(5)	2.077(4)
Co-N$_{amine}$	1.978(1) 1.987(1)	2.251(3)	2.351(5) – 2.461(5)	2.407(4)
Co-Cl	2.255(1) 2.264(1)	2.401(1)	2.358(2) – 2.405(2)	2.365(3) – 2.403(2)
N$_{py}$-Co-N$_{py}$	89.8(1)	79.6(1)	82.6(1) – 83.4(1)	83.1(2)
N$_{amine}$-Co-N$_{amine}$	163.3(1)	148.2(1)	140.3(1) – 141.4(1)	141.4(2)
Cl-Co-Cl	91.5(1)	97.8(1)	93.7(1) – 96.7(1)	97.9(1)
CCDC ref./no.	1892441	ZAKHIC	ACISUA	XACHAL
Reference	this work	[19]	[21]	[23]

LN4H$_2$ = 2,11-diaza[3,3](2,6)pyridinophane

LN4Me$_2$ = *N,N'*-dimethyl-2,11-diaza[3,3](2,6)pyridinophane

LN4^{t}Bu$_2$ = *N,N'*-di-*tert*-butyl-2,11-diaza[3,3](2,6)pyridinophane

[a]values are averaged when they are identical within 3σ, otherwise the range of values is given; the error was calculated using the formula for propagation of error in calculations

Table S9. Comparison of averaged[a] bond distances (Å) and angles (º) in **3^{Ni}** with those in selected relevant complexes [Ni^{II}(**L**)(μ-Cl)]$_2$X$_2$ (**L** = tetradentate aminopyridiyl and tetraaza κ^{4}N type ligands) and [Ni(**LN4R$_2$**)X$_2$]^n (**LN4R$_2$** = diazapyridinophane type ligands)

Compound	**3^{Ni}** {[Ni^{II}(**LN4H$_2$**)(μ-Cl)]$_2$Cl$_2$ • solvent	{[Ni^{II}(**L1**)(μ-Cl)]$_2$Cl$_2$ • solvent	{[Ni^{II}(**L2**)(μ-Cl)]$_2$(ClO$_4$)	[Ni^{II}(**LN4Me$_2$**)(H$_2$O)Cl]Cl • H$_2$O	Ni^{II}(**LN4^{t}Bu$_2$**)Cl$_2$ • solvent
Ni-N$_{eq}$	Ni-N$_{eq}$ = Ni-N$_{py}$ 2.008(3)	Ni-N$_{eq}$ = Ni-N$_{py}$ 1.997(2) Ni-N$_{eq}$ = Ni-N$_{amine}$ 2.077(2)	Ni-N$_{eq}$ = Ni-N$_{amine}$ 2.103(4)	Ni-N$_{eq}$ = Ni-N$_{py}$ 2.022(3)	Ni-N$_{eq}$ = Ni-N$_{py}$ 2.008(4) – 2.022(7)
Ni-N$_{axial}$	Ni-N$_{axial}$ = Ni-N$_{amine}$ 2.155(3)	Ni-N$_{axial}$ = Ni-N$_{amine}$ 2.129(1)	Ni-N$_{axial}$ = Ni-N$_{amine}$ 2.041(4)	Ni-N$_{axial}$ = Ni-N$_{amine}$ 2.199(3)	Ni-N$_{axial}$ = Ni-N$_{amine}$ 2.292(5) – 2.337(5)
Ni-Cl	2.405(1) 2.414(1)	2.383(1) (*trans* N$_{py}$) 2.462(1) (*trans* N$_{amine}$)	2.551(1) (*trans* N$_{amine}$)	2.383(2) (*trans* N$_{py}$)	2.356(1) – 2.396(1) (*trans* N$_{py}$)
N$_{eq}$-Ni-N$_{eq}$	N$_{py}$-Ni-N$_{py}$ 89.0(1)	N$_{amine}$-Ni- N$_{py}$ 95.7(1)	N$_{amine}$-Ni-N$_{amine}$ 94.4(2)	N$_{py}$-Ni-N$_{py}$ 82.6(2)	N$_{py}$-Ni-N$_{py}$ 85.3(1) – 87.4(2)
N$_{axial}$-Ni-N$_{axial}$	N$_{amine}$-Ni-N$_{amine}$ 152.9(1)	N$_{amine}$-Ni-N$_{amine}$ 155.5(1)	N$_{amine}$-Ni-N$_{amine}$ 166.2(2)	N$_{amine}$-Ni-N$_{amine}$ 154.1(1)	N$_{amine}$-Ni-N$_{amine}$ 146.2(1)
Cl-Ni-Cl	87.5(1)	85.0(1)	75.9(1)	92.5(1) (Cl-Ni-O)	92.7(1) – 93.3(1)
Ni-Cl-Ni	92.5(1)	95.0(1)	104.1(1)	-	-
Ni···Ni	3.48(1)	3.57(1)	4.02(1)	-	-
CCDC ref./no.	1892443	EFOTAW	MEJGIR	ZAKHEY	HICRAO
Reference	this work	[24]	[25]	[19]	[22]

LN4H$_2$ = 2,11-diaza[3,3](2,6)pyridinophane
LN4Me$_2$ = *N,N'*-dimethyl-2,11-diaza[3,3](2,6)pyridinophane
LN4^{t}Bu$_2$ = *N,N'*-di-*tert*-butyl-2,11-diaza[3,3](2,6)pyridinophane
L1 = 3,6,9,15-tetraazabicyclo[9.3.1]pentadeca-1(15),11,13-triene
L2 = [2^4.3^1]adamanzane = 1,4,7,10-tetraazabicyclo[5.5.3]pentadecane
[a]values are averaged when they are identical within 3σ, otherwise the range of values is given; the error was calculated using the formula for propagation of error in calculations

Table S10. Comparison of averaged[a] bond distances (Å) and angles (º) in **4^{Zn}** with those in selected relevant monomeric complexes [Zn(**LN4R$_2$**)X$_2$]^n (**LN4R$_2$** = diazapyridinophane type ligands)

Compound	**4^{Zn}** Zn^{II}(**LN4H$_2$**)Cl_2 • solvent	Zn^{II}(**LN4Me$_2$**)Cl_2 • $2H_2O$	Zn^{II}(**LN4^{t}Bu$_2$**)(NCMe)(OTf)](OTf) • CH_3CN
Zn-N_{py}	2.128(1)	2.173	2.028(2) 2.050(2)
Zn-N_{amine}	2.276(1)	2.304	2.307(2) 2.365(2)
Zn-Cl	2.386(1)	*n.r*	-
Zn-O	-	-	2.135(2)
N_{py}-Zn-N_{py}	81.0(1)	76.8	88.6(1)
N_{amine}-Zn-N_{amine}	144.3(1)	144	144.9(1)
Cl-Zn-Cl	93.5(1)	*n.r*	-
N_{NCMe}-Zn-O	-	-	85.6(1)
CCDC ref./no.	1892444	*n.r*	HICQOB
Reference	this work	[19]	[22]

LN4H$_2$ = 2,11-diaza[3,3](2,6)pyridinophane

LN4Me$_2$ = *N,N'*-dimethyl-2,11-diaza[3,3](2,6)pyridinophane

LN4^{t}Bu$_2$ = *N,N'*-di-*tert*-butyl-2,11-diaza[3,3](2,6)pyridinophane

[a]values are averaged when they are identical within 3σ, otherwise the range of values is given; the error was calculated using the formula for propagation of error in calculations

n.r. = not reported

Table S11. H-bonding geometry for compounds $\mathbf{1^{Fe}}$ – $\mathbf{4^{Zn}}$. Distances are in (Å) and angles in (°).

***D*—H···*A* (type*)**	***D*—H**	**H···*A***	***D*···*A***	***D*—H···*A***
		1^{Fe}		
N2—H2···Cl3[1]	0.94(5)	2.31(5)	3.22(1)	162(4)
N4—H4···Cl3	0.87(5)	2.48(5)	3.27(1)	150(4)
N8—H8···Cl3[1]	0.85(5)	2.47(5)	3.24(1)	150(4)
C2—H2A···Cl4	0.95	2.78	3.62(1)	147
C4—H4A···Cl4[1]	0.95	2.87	3.71(1)	148
C9—H9···Cl1[2]	0.95	2.94	3.68(1)	136
C11—H11···Cl1[3]	0.95	2.85	3.62(1)	139
C18—H18···Cl4[4]	0.95	2.96	3.78(1)	145
C20—H20A···Cl3	0.99	2.70	3.67(1)	166
C27—H27B···Cl4[5]	0.99	2.73	3.65(1)	155
Symmetry codes: [1]-1+X, +Y, +Z; [2]-X, 1-Y, 1-Z; [3]1-X, 1-Y, 1-Z; [4]+X, -1+Y, +Z; [5]-1+X, -1+Y, +Z				
		2^{Co}		
N2—H2···Cl2[1]	0.90(3)	2.41(3)	3.28(1)	161(2)
N4—H4A···Cl1[3]	0.88(3)	2.46(3)	3.23(1)	146(2)
C4—H4···Cl3[2]	0.95	2.71	3.56(1)	150
C6—H6A···Cl3[2]	0.99	2.99	3.65(1)	126
C9—H9···Cl2[4]	0.95	2.97	3.64(1)	129
C13—H13A···Cl2[3]	0.99	2.83	3.75(1)	154
C13—H13B···Cl3[5]	0.99	2.72	3.62(1)	151
C14—H14A···Cl3[5]	0.99	2.56	3.43(1)	147
C14—H14B···Cl3[6]	0.99	2.77	3.57(1)	138
Symmetry codes: [1]1-X, -Y, -Z; [2]1-X, 1-Y, 1-Z; [3]-X, -Y, -Z; [4]+X, 1+Y, +Z; [5]-X, 1-Y, 1-Z; [6]+X, -1+Y, +Z				
		3^{Ni}		
N2—H2···Cl2	0.80(6)	2.43(6)	3.23(1)	173(5)
C2—H2A···Cl3	0.95	2.94	3.65(1)	133
C4—H4B···Cl3	0.99	2.80	3.72(1)	153
		4^{Zn}		
N2—H2···Cl1[1]	0.87(2)	2.64(2)	3.41(1)	148(1)
N2—H2···Cl1[2]	0.87(2)	2.98(2)	3.62(1)	132(1)
C7—H7B···Cl1[2]	0.99	2.76	3.58(1)	140
Symmetry codes: [1]-1/2+X, 3/4-Y ,5/4-Z; [2]5/4-X, +Y, 5/4-Z				

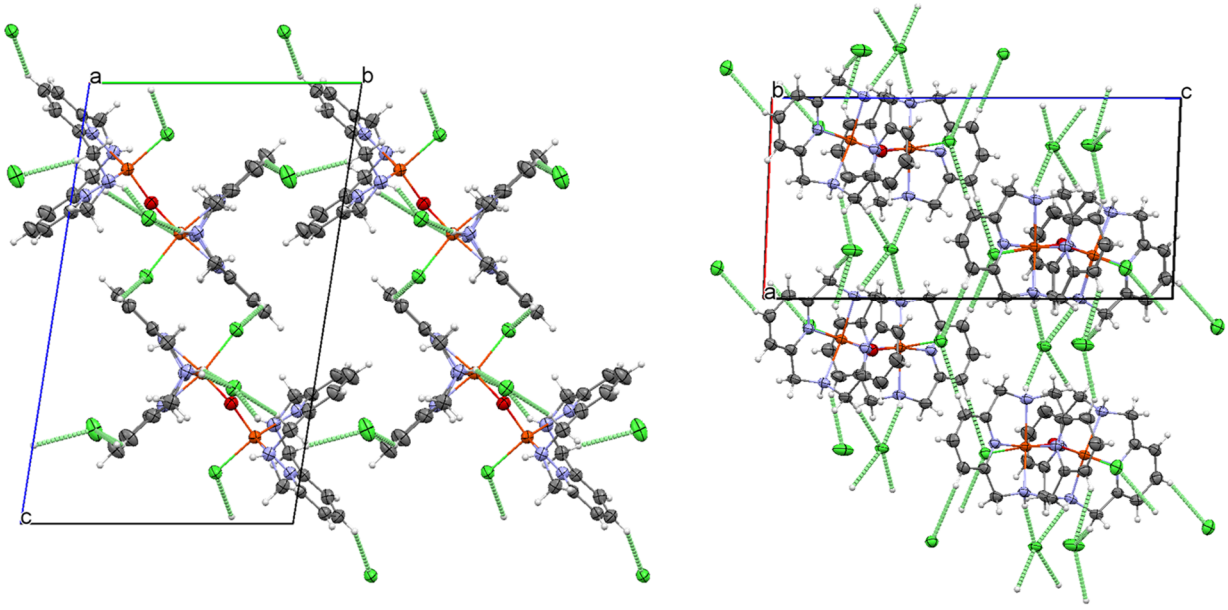

Fig. S6. The solid state structure of $\mathbf{1}^{Fe}$ – H-bonding pattern along *a* axis (left) and *b* axis (right) – ORTEP views at 50% probability level.

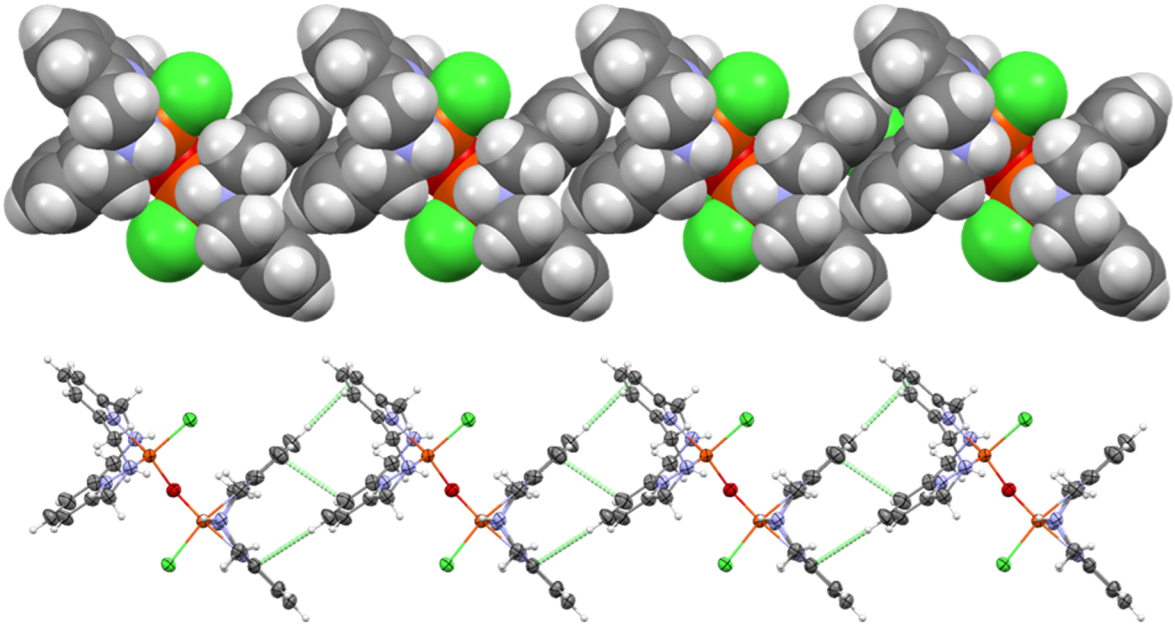

Fig. S7. π – π and π – H-C(sp^2) intermolecular packing interactions in the solid state structure of $\mathbf{1}^{Fe}$ – spacefill view (top) and ORTEP view at 50% probability level (bottom).

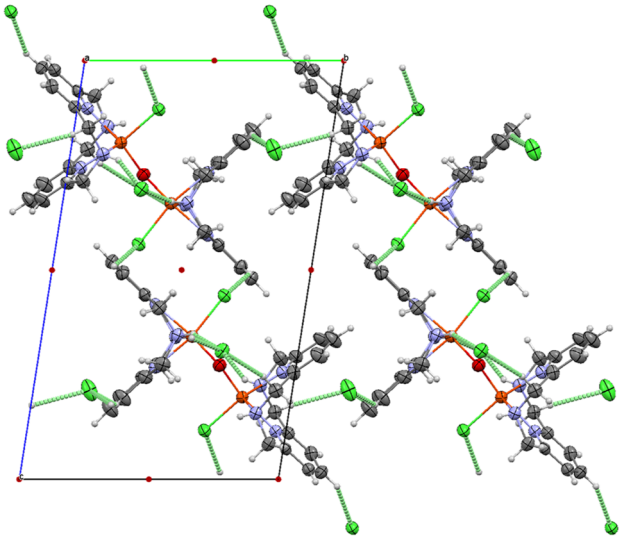

Fig. S8. The solid state structure of **2**^{Co} – H-bonding pattern along *a* axis – ORTEP view at 50% probability level.

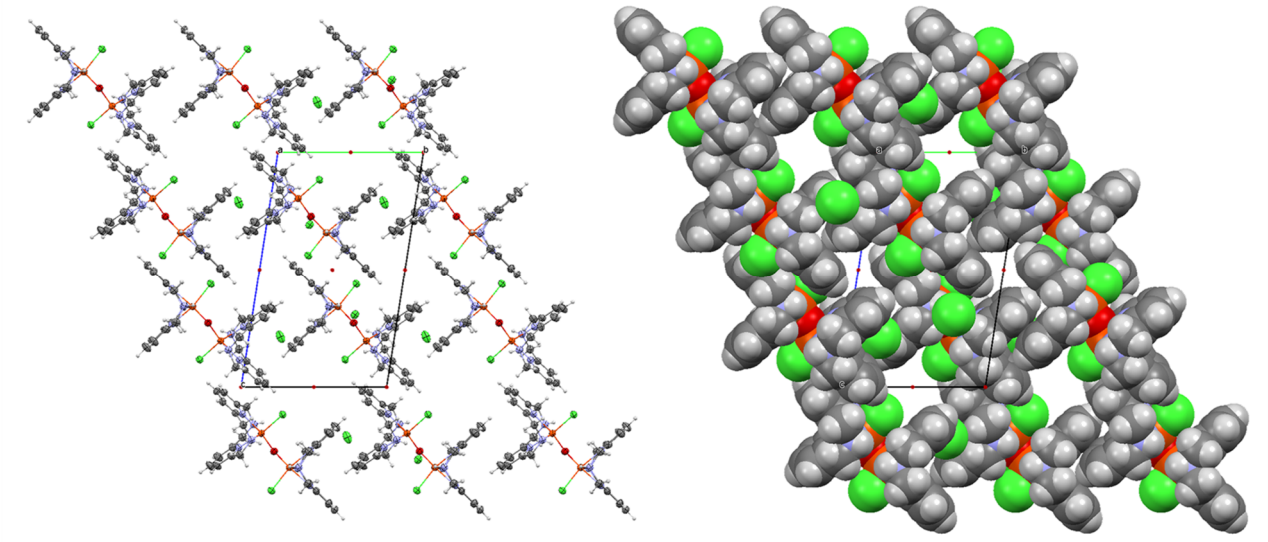

Fig. S9. The solid state structure of **2**^{Co} – packing pattern: view along *a* axis – ORTEP view at 50% probability level (left) and specefill view (right).

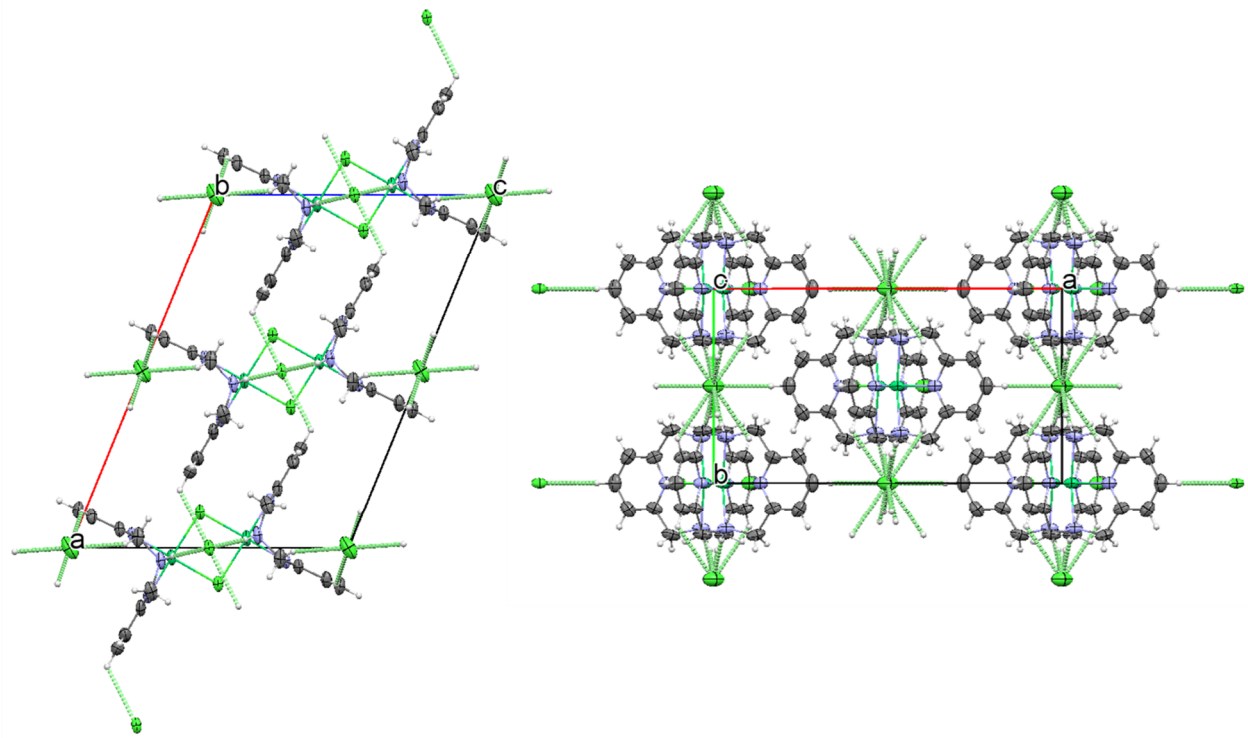

Fig. S10. The solid state structure of **3**^{Ni} – packing and H-bonding patterns: view along *b* axis (left) and view along *c* axis (right) – ORTEP views at 50% probability level.

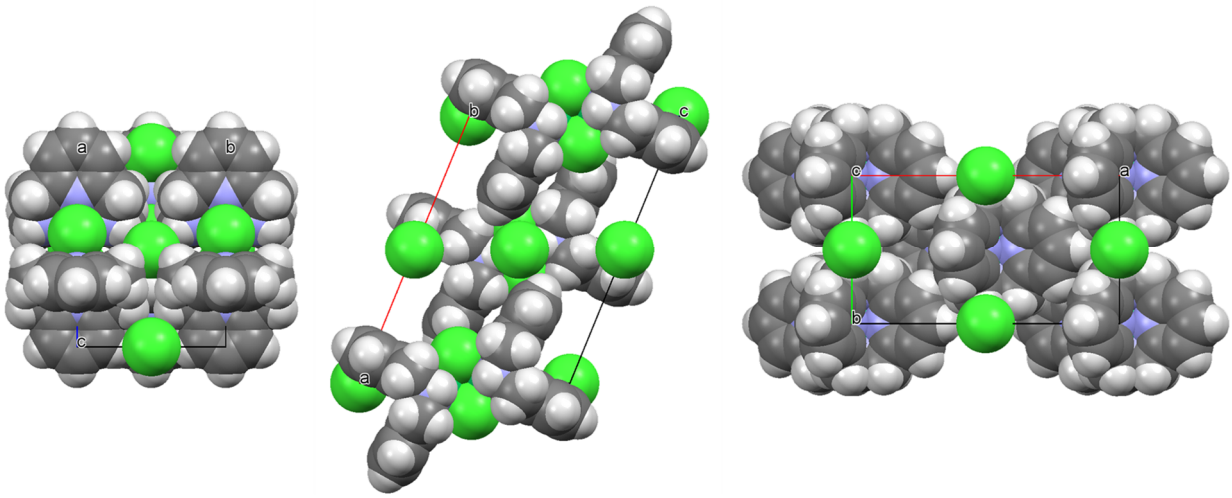

Fig. S11. The solid state structure of **3**^{Ni} – packing pattern along *a* axis (left), *b* axis (middle), and *c* axis (right) – spacefill views.

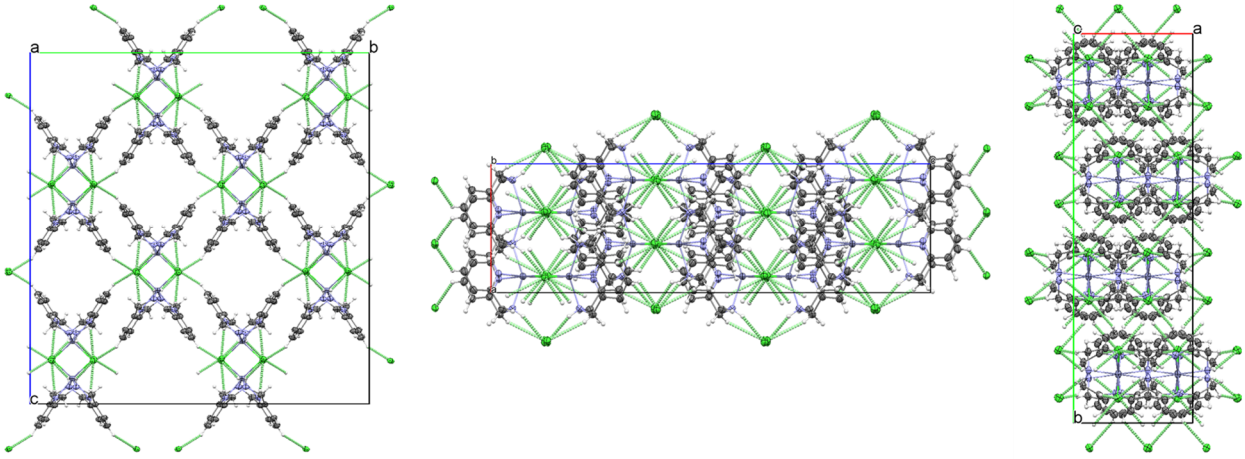

Fig. S12. The solid state structure of **4**^{Zn} – packing and H-bonding patterns along *a* axis (left), *b* axis (middle), and *c* axis (right) – ORTEP views at 50% probability level.

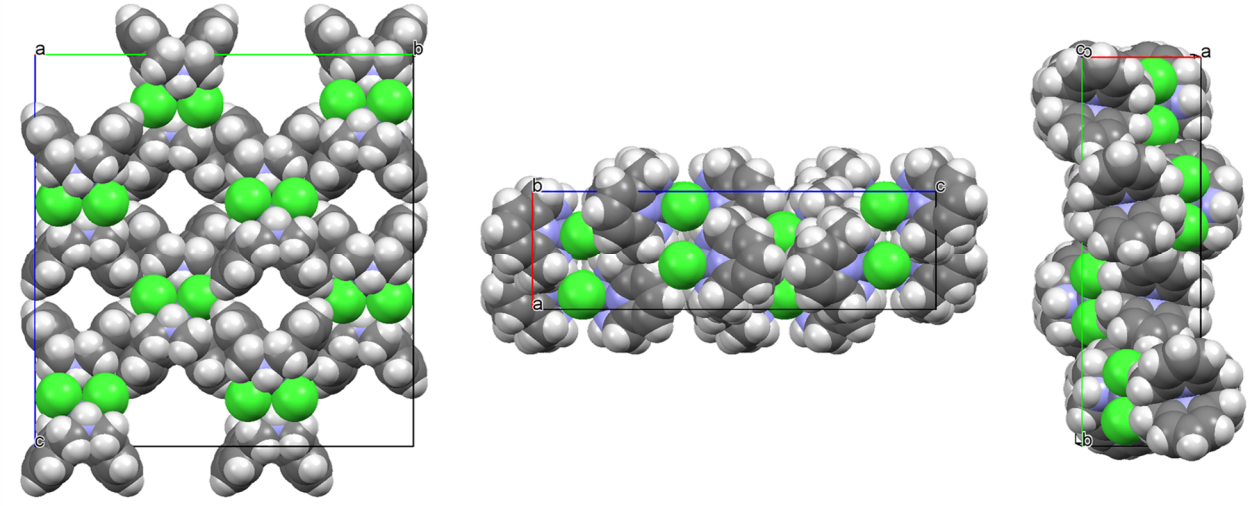

Fig. S13. The solid state structure of **4**^{Zn} – packing pattern along *a* axis (left), *b* axis (middle), and *c* axis (right) – spacefill views.

Electronic absorption spectroscopy

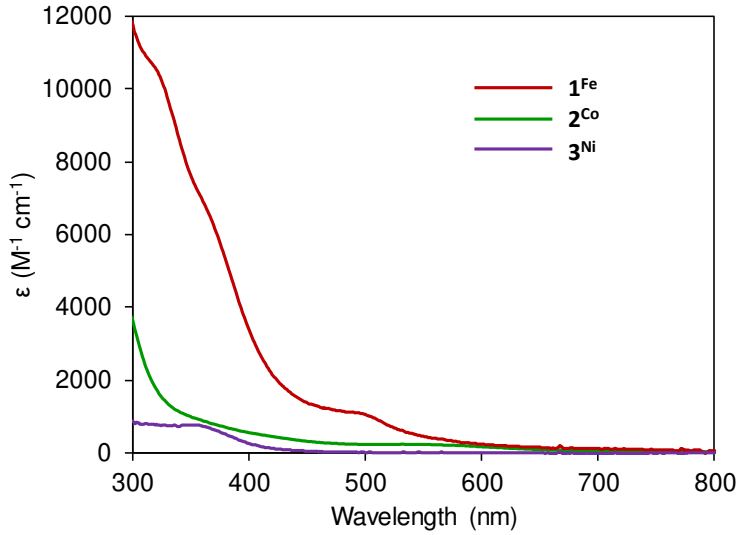

Fig. S14. UV-vis spectra of a DMF solution of $\mathbf{1}^{Fe}$, $\mathbf{2}^{Co}$ and $\mathbf{3}^{Ni}$.

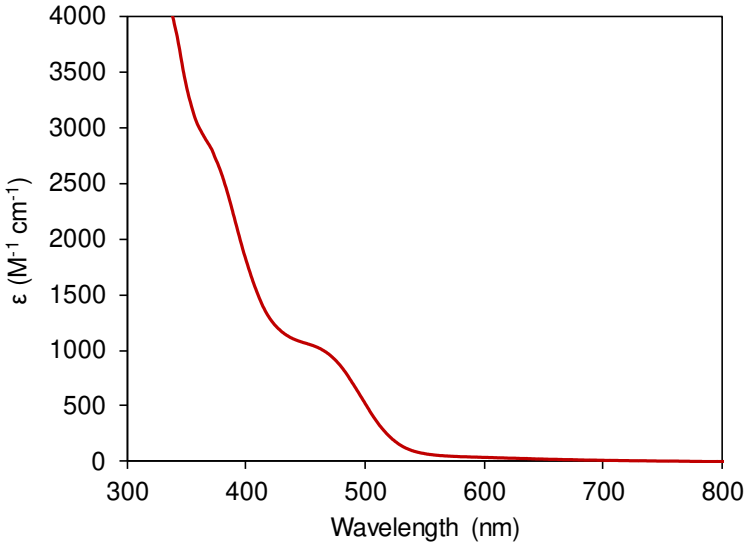

Fig. S15. UV-vis spectra of a DMF solution of $\mathbf{1}_{m}^{Fe}$.

FTIR spectroscopy

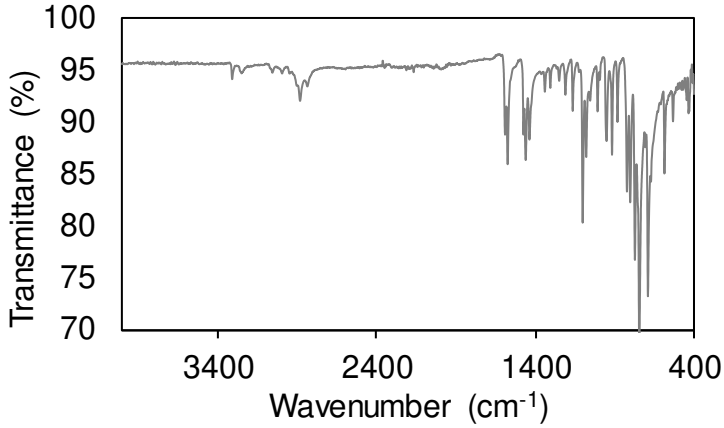

Fig. S16. IR spectra of **LN4H$_2$**.

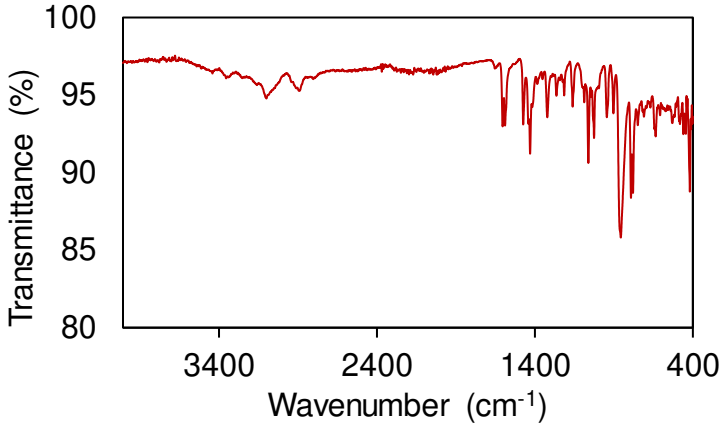

Fig. S17. IR spectra of **1^{Fe}**.

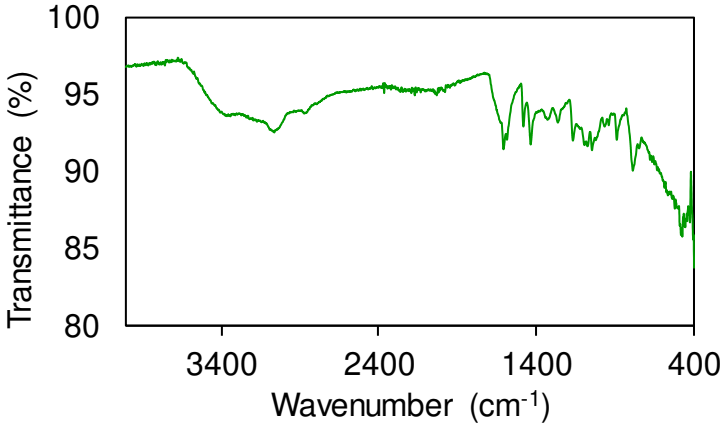

Fig. S18. IR spectra of **2^{Co}**.

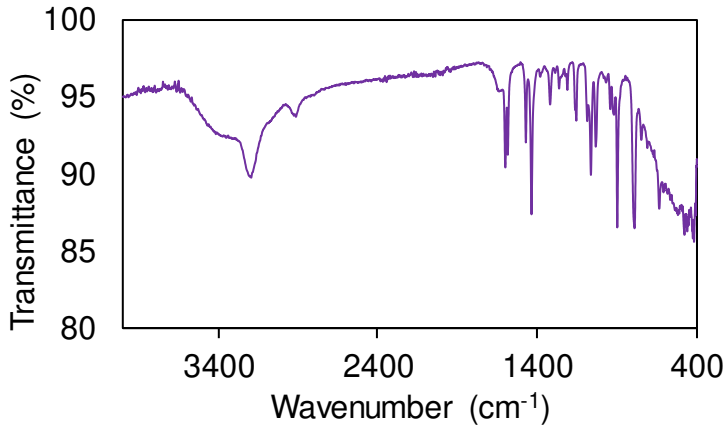

Fig. S19. IR spectra of $\mathbf{3^{Ni}}$.

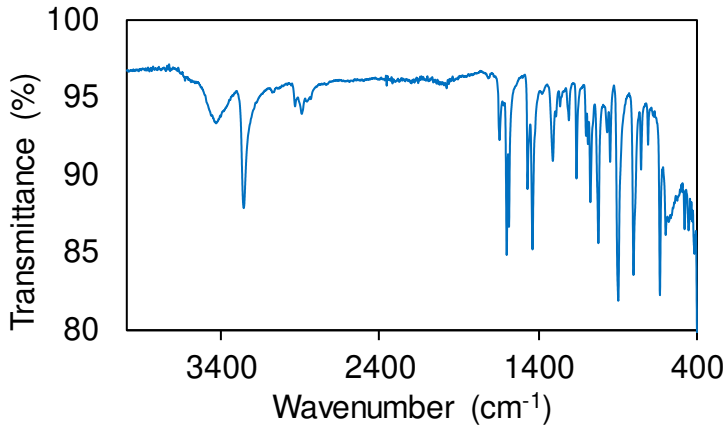

Fig. S20. IR spectra of $\mathbf{4^{Zn}}$.

^{1}H-NMR spectroscopy

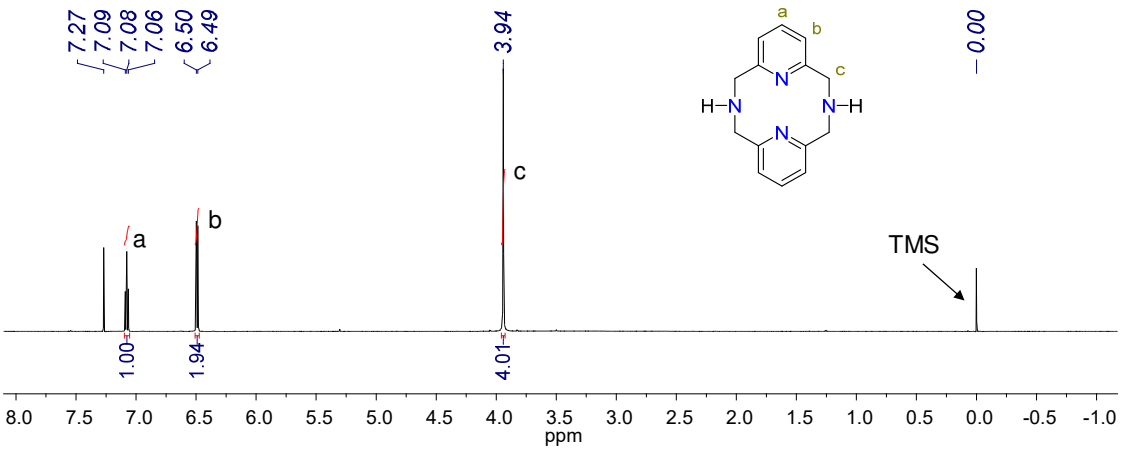

Fig. S21. ^{1}H NMR ($CDCl_3$, 600 MHz, 293 K) spectra of **LN4H$_2$**.

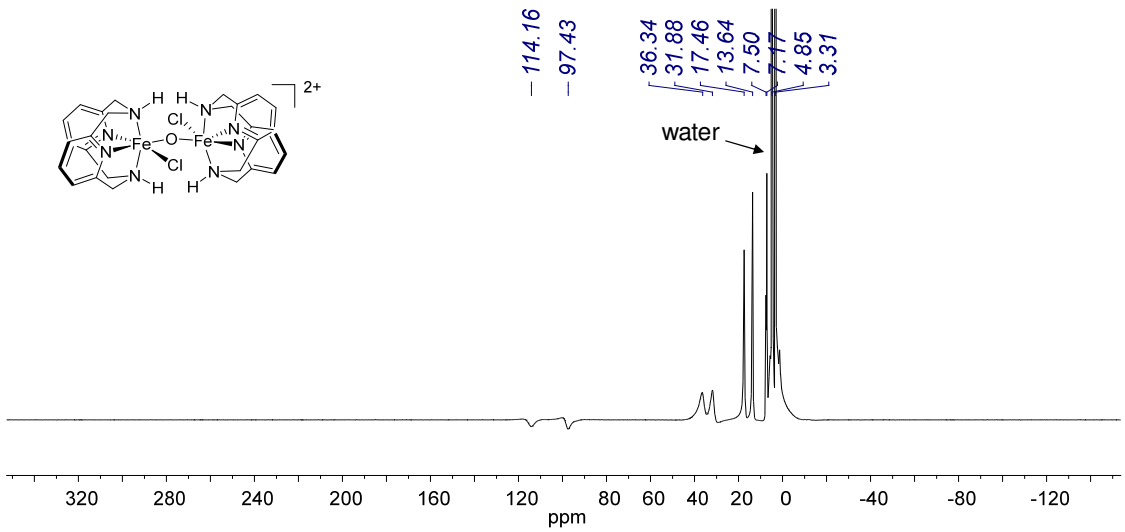

Fig. S22. ^{1}H NMR (CD_3OD, 600 MHz, 293 K) spectra of $\mathbf{1^{Fe}}$.

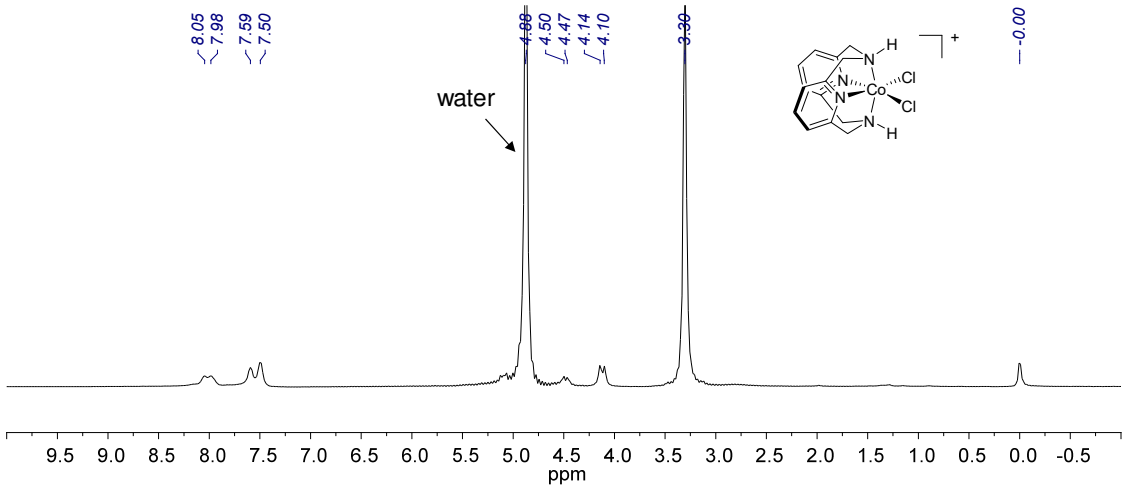

Fig. S23. ^{1}H NMR (CD_3OD, 600 MHz, 293 K) spectra of $\mathbf{2^{Co}}$.

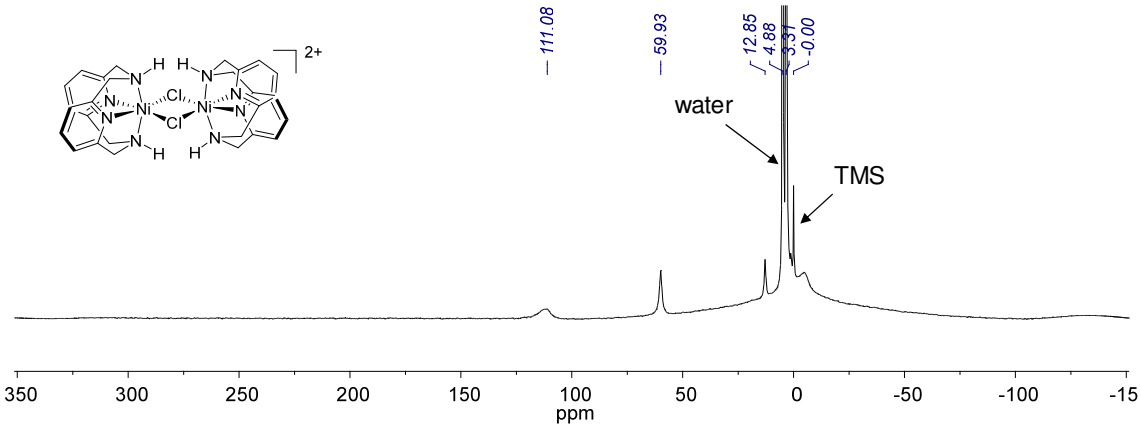

Fig. S24. ^{1}H NMR (CD_3OD, 400 MHz, 293 K) spectra of $\mathbf{3^{Ni}}$.

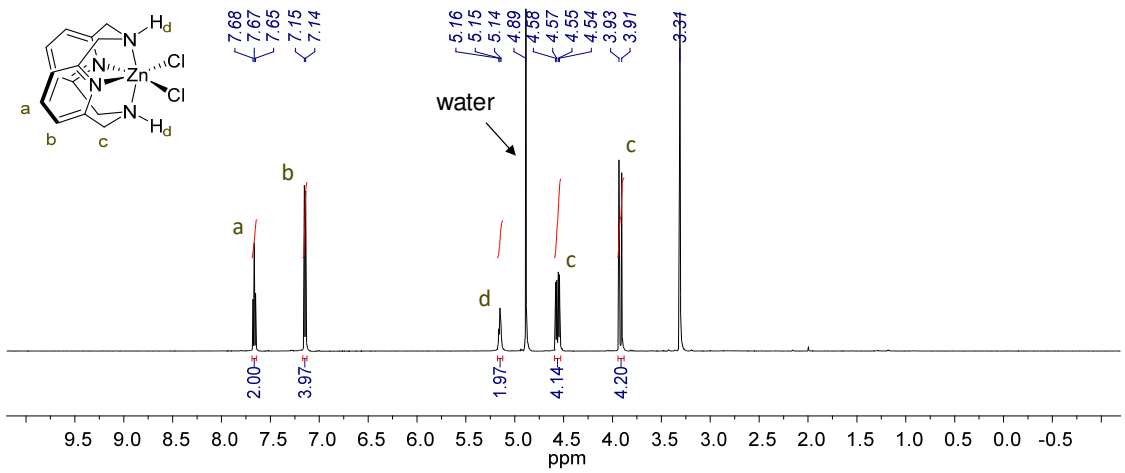

Fig. S25. ^{1}H NMR (CD_3OD, 600 MHz, 293 K) spectra of $\mathbf{4^{Zn}}$.

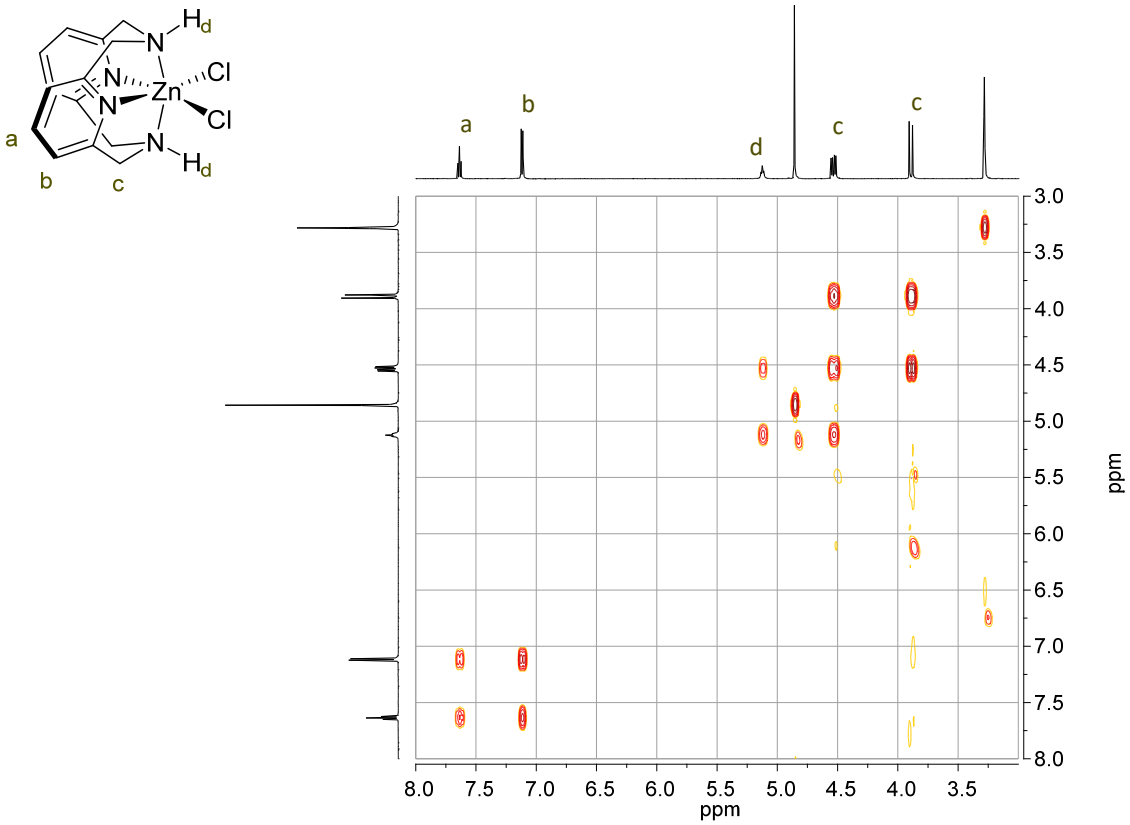

Fig. S26. ^{1}H-^{1}H COSY (CD_3OD, 600 MHz, 293 K) spectra of $\mathbf{4^{Zn}}$.

8. Spectrophotometric experiments

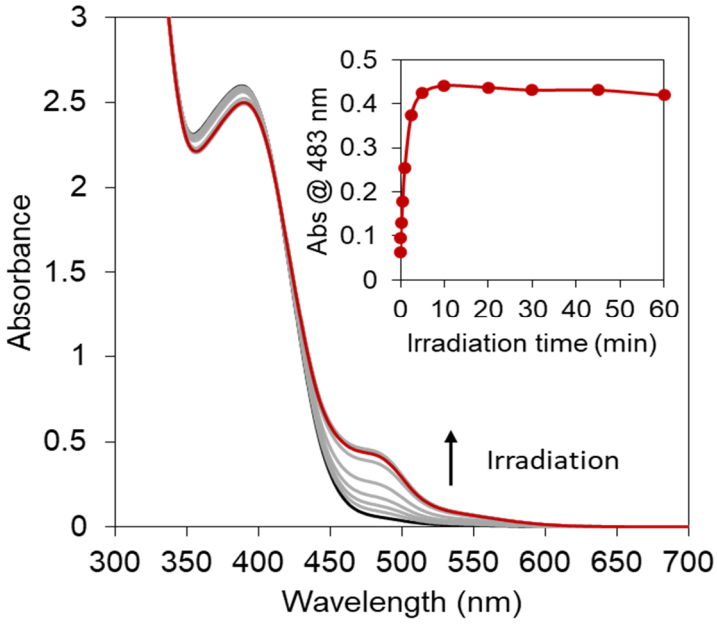

Fig. S27. UV/Vis spectral changes of a 0.5 mM solution of **Cu-PS** in DMF during irradiation showing the formation of the homoleptic $[Cu(N^N)_2]^+$ at 483 nm.

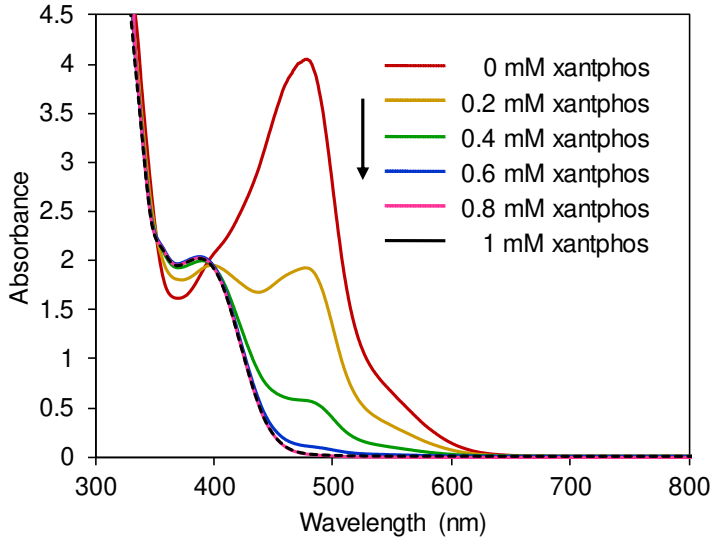

Fig. S28. UV/Vis spectral changes of a 0.28 mM (calculated from ε_{max}@479 nm) DMF:TEOA (4:1 *v/v*) solution of the homoleptic complex $[Cu(bathocuproine)_2]^+$ ($[Cu(N^N)_2]^+$) upon addition of xantphos (P^P). The formation the heteroleptic complex $[Cu(P^P)(N^N)]^+$ is clearly shown.

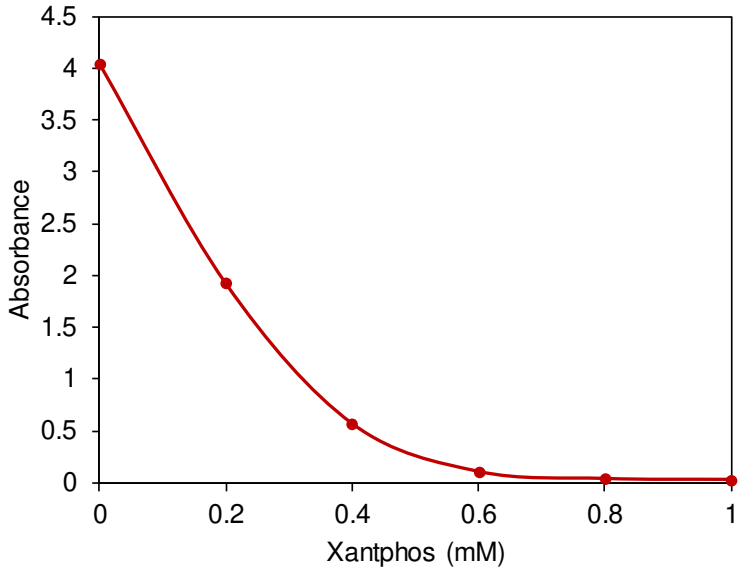

Fig. S29. Plot of the absorbance at 389 nm of a 0.28 mM solution of $[Cu(N\hat{}N)_2]^+$ at different concentration of addition of xantphos.

9. Quantum yield determination

The internal quantum yield (IQY) for CO formation (Φ_{CO}) was calculated using the following equation;

$$\Phi = \frac{\text{Number of CO molecules} \times 2}{\text{Number of photons absorbed}} \times 100$$

The number of CO molecules was determined from the moles of CO in the sample headspace (determined by GC measurements). The number of photons absorbed by the system (1.15×10^{20} photons) was estimated from the irradiated light passed through a cut-off filter (L40 and B370, HOYA, $350 < \lambda < 500$ nm) by using a grating spectroradiometer (LS 100, EKO Instruments) (Fig. S30).

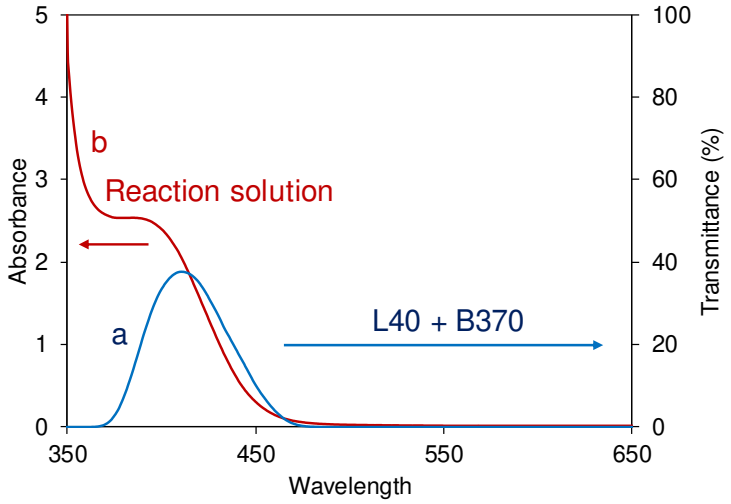

Fig. S30 *a)* Transmittance of the employed combination of glass filters (L40 + B370, HOYA). *b)* UV-vis absorption the reaction mixture containing **1**^{Fe} (0.05 mM), **Cu-PS** (0.5 mM), xantphos (1 mM) in the presence of BIH (50 mM) in a DMF:TEOA (4:1 *v/v*) solution.

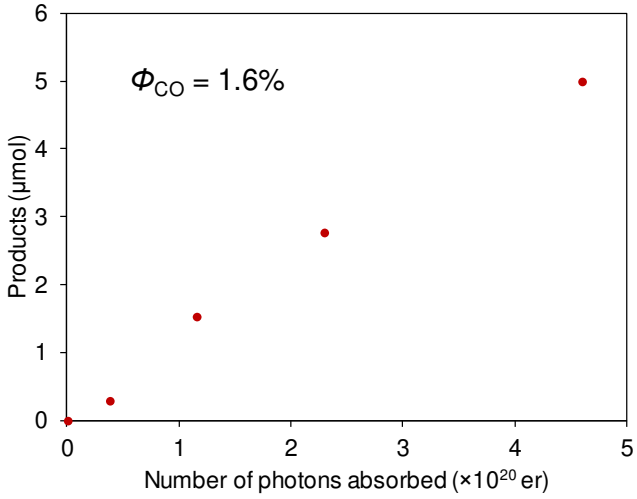

Fig. S31 The amount of CO produced as a function of the number of photons absorbed. Conditions: **1**^{Fe} (0.05 mM), **Cu-PS** (0.5 mM), xantphos (1 mM) in the presence of BIH (50 mM) in a DMF:TEOA (4:1 *v/v*) solution, T = 25 ºC, using a photoirradiation in the 350-500 nm domain using the set of glass filters described in Fig.S30.

10. Photocatalytic reactions

Table S12. Control experiments.

Entry	$\mathbf{1}^{Fe}$ (mM)	**Cu-PS** (mM)	BIH (mM)	Product (μmol)		Sel_{CO2} (%)
				CO	H_2	
1[a]	0.025	0.5	50	65.7	37.4	63
2	0.025	0.5	50	141.3	29.0	84
3	0	0.5	50	6.5	24.0	21
4	0.025	0	50	N. D.	N. D.	N. D.
5	0.025	0.5	0	0.3	7.3	4
6[b]	0.025	0.5	50	N. D.	26.0	0
7[c]	0.025	0.5	50	4.7	4.2	53

All reactions performed in a 5 mL CO_2-saturated DMF:TEOA (4:1 *v*/*v*) solution containing 1 mM xantphos unless otherwise indicated. [a] In the absence of xantphos. [b] Photocatalytic experiment performed under N_2. [c] TEA was used instead of TEOA.

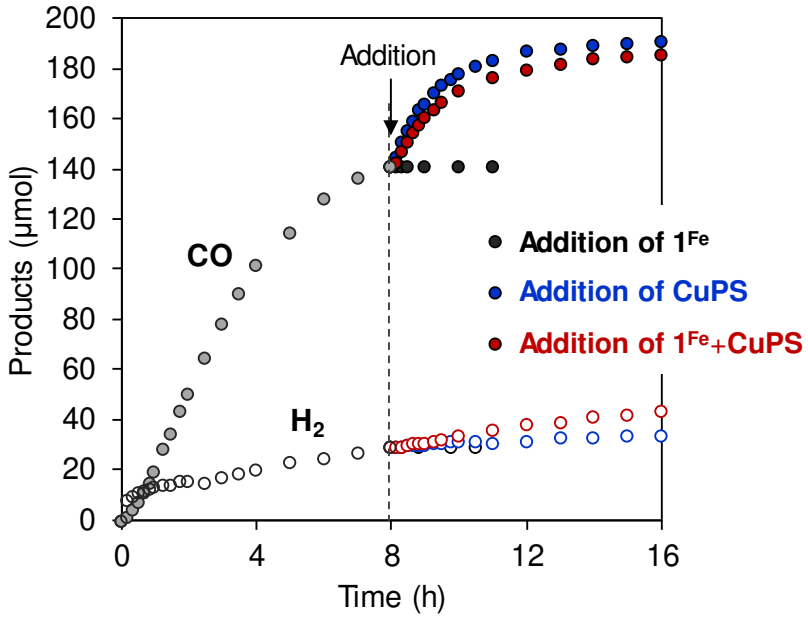

Fig. S32. Addition experiments: recovery of CO (dots) and H_2 (empty circles) production upon addition of $\mathbf{1}^{Fe}$ (0.025 mM) and/or **Cu-PS** (0.5 mM) to a DMF:TEOA (4:1 v/v) solution containing $\mathbf{1}^{Fe}$ (0.025 mM), **Cu-PS** (0.5mM), xantphos (1 mM), and BIH (50 mM) under visible light irradiation at T = 25 ºC.

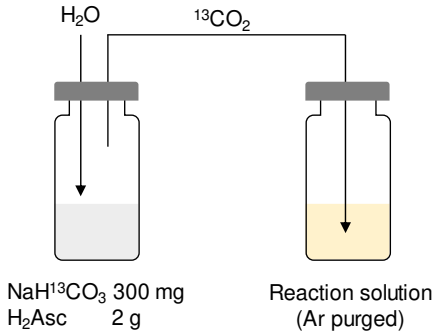

Fig. S33 The $^{13}CO_2$ labeling experiments were performed using 5 mL of a DMF:TEOA (4:1) solution containing **1^{Fe}** (0.05 mM), **Cu-PS** (0.5 mM), xantphos (1 mM), and BIH (50 mM). The reaction vessel was purged with Ar for 15 min, followed by $^{13}CO_2$ bubbling. As shown in the figure, the $^{13}CO_2$ gas was produced by adding water to a mixture of ascorbic acid with $NaH^{13}CO_3$ (99 atom % ^{13}C, Cambridge Isotope Laboratories, Inc).

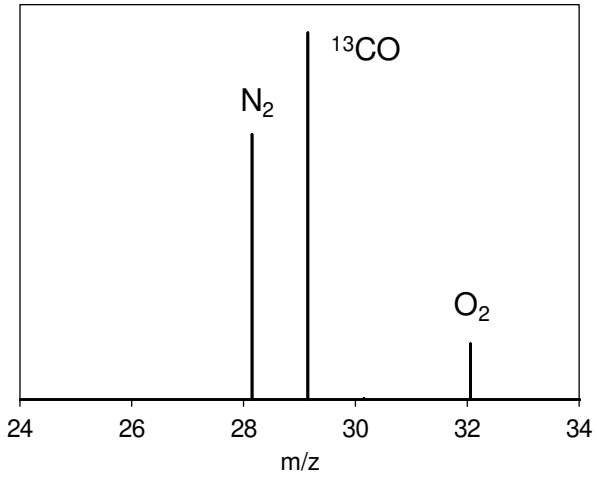

Fig. S34 Mass spectra of CO generated under $^{13}CO_2$. Isotope labelling experiments were carried out in a 5 mL CO_2-saturated solution containing **1^{Fe}** (0.05 mM), **Cu-PS** (0.5 mM), xantphos (1 mM) in the presence of BIH (50 mM) in a DMF:TEOA (4:1 *v/v*) solution, T = 25 ºC, using Xe lamp irradiation (λ > 400 nm, 179 mW·cm^{-2}).

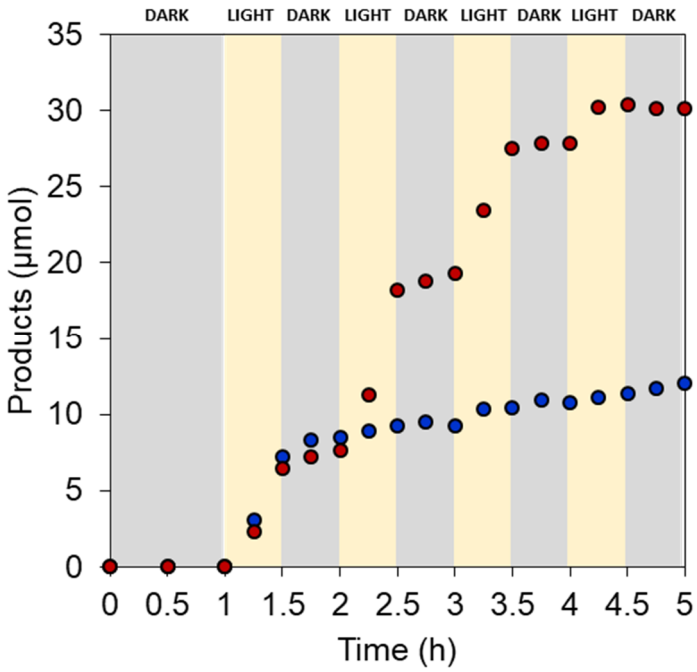

Fig. S35. Light-dark cycles for the photocatalytic generation of CO (red dots) and H_2 (blue dots). Conditions: Photolysis was carried put in a 5 mL CO_2-saturated solution of DMF:TEOA (4:1 *v/v*) containing **1**^{Fe} (0.05 mM in Fe), **Cu-PS** (0.5 mM), BIH (50 mM), xantphos (1 mM), T = 25 ºC, using Xe lamp irradiation (λ > 400 nm, 179 mW·cm^{-2}).

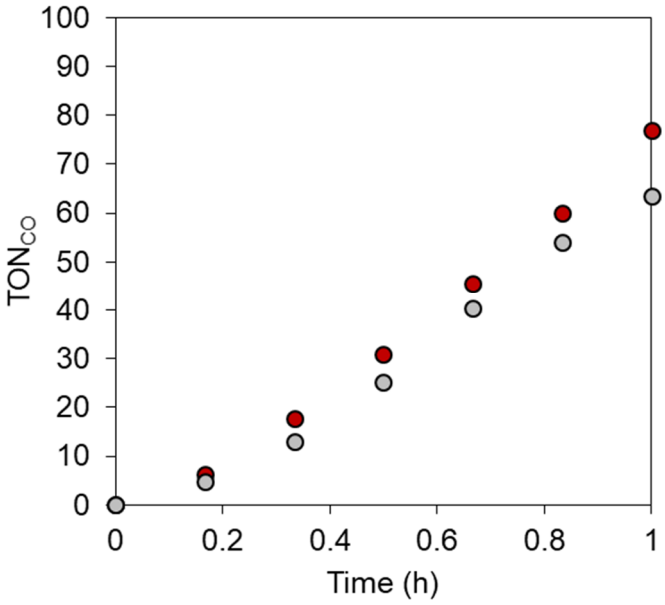

Fig. S36. Photocatalytic activities in CO production in the presence (grey dots) and absence (red dots) of Hg(0) (1g, 20000 eq. *vs.* Fe center). Conditions: Photolysis was carried out in a 5 mL CO_2-saturated solution of DMF:TEOA (4:1 *v/v*) containing **1**^{Fe} (0.05 mM in Fe), **Cu-PS** (0.5 mM), BIH (50 mM), xantphos (1 mM), T = 25 ºC, using Xe lamp irradiation (λ > 400 nm, 179 mW·cm^{-2}).

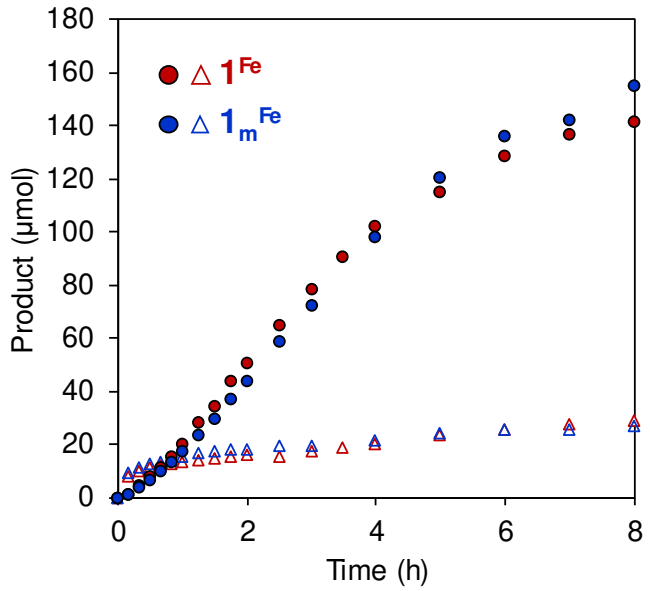

Fig. S37. Time courses of CO (dots) and H_2 (triangles) produced using $\mathbf{1}^{Fe}$ (red) and $\mathbf{1_m}^{Fe}$ (0.05 mM), **Cu-PS** (0.5 mM) in the presence of BIH (50 mM) in a DMF:TEOA (4:1 *v/v*) solution, T = 25 ºC, using Xe lamp irradiation (λ > 400 nm, 179 mW·cm^{-2}).

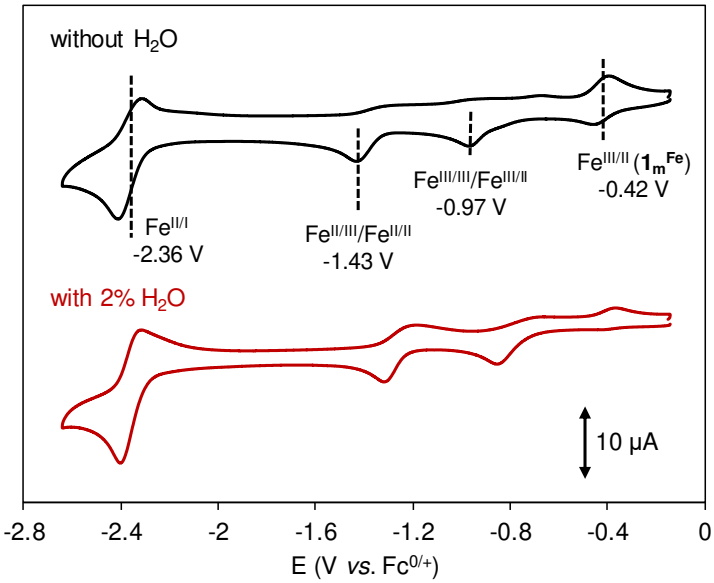

Fig. S38. CV of a 1 mM DMF solution of $\mathbf{1}^{Fe}$ at 100 mV·s^{-1} under Ar in the presence and absence of water (GC working electrode, 0.1 M Bu_4NPF_6). When water is absent in solution, the peak at -0.42 V corresponding to the $Fe^{III/II}$ couple of $\mathbf{1_m}^{Fe}$ can be observed, confirming that the monomeric $\mathbf{1_m}^{Fe}$ complex is formed upon dissolving $\mathbf{1}^{Fe}$ in DMF.

11. Mechanistic experiments

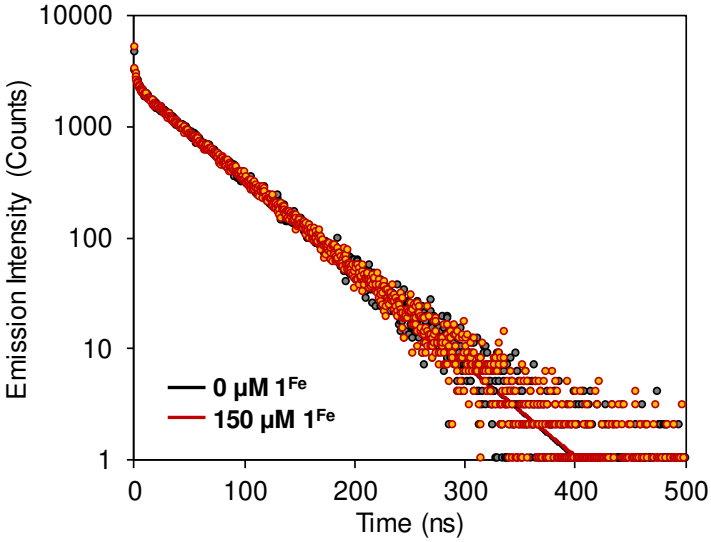

Fig. S39. Emission decay of **Cu-PS** (0.5 mM) in DMF under Ar atmosphere, in the presence and absence of **1^{Fe}** catalyst, viewed as a logarithmic plot of the emission intensity at 552 nm. The initial rapid decay is attributed to structural changes. The lines are single exponential fits.

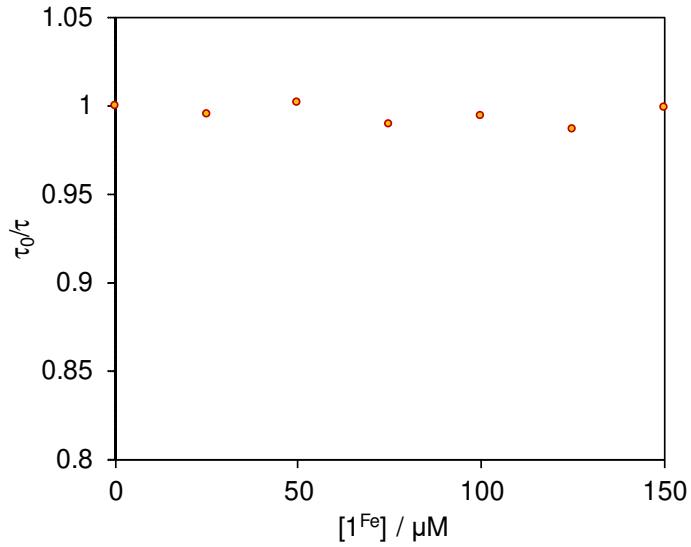

Fig. S40. Stern-Volmer plot for the quenching of **Cu-PS*** by **1^{Fe}** measured in DMF:TEOA (4:1 *v*/*v*).

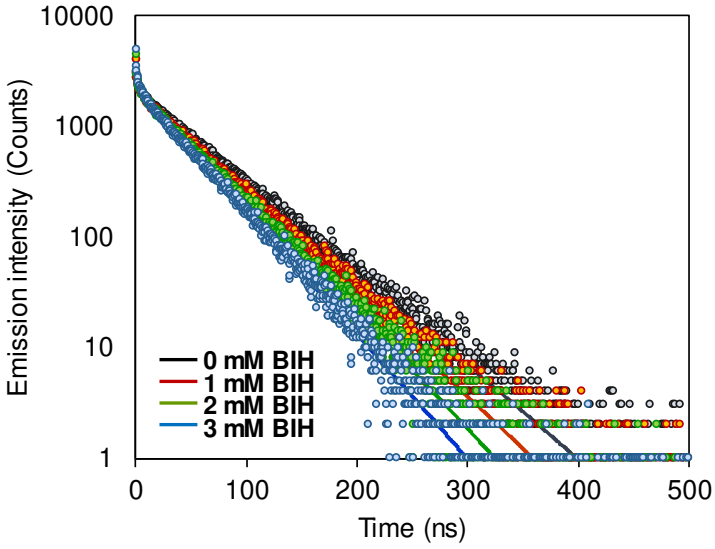

Fig. S41. Emission decay of **Cu-PS** (0.5 mM) in DMF:TEOA (4:1 *v*/*v*) in the presence of xantphos (1 mM) under Ar atmosphere at different concentrations of BIH, viewed as a logarithmic plot of the emission intensity at 552 nm. The initial rapid decay is attributed to structural changes. The lines are single exponential fits.

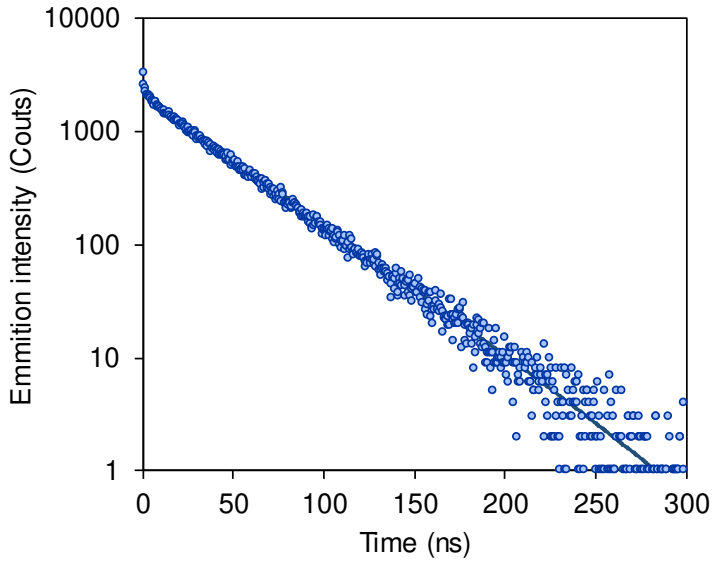

Fig. S42. Emission decay of **Cu-PS** (0.5 mM) in DMF under Ar atmosphere, viewed as a logarithmic plot of the emission intensity at 552 nm. The initial rapid decay is attributed to structural changes. The line is a single exponential fits. The lifetime (τ) is estimated as τ = 37 ns.

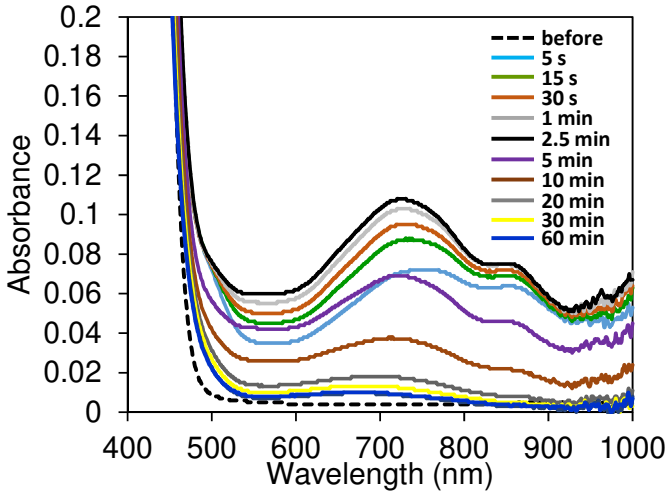

Fig. S43. UV/Vis spectral changes for **Cu-PS** obtained during irradiation in the presence of BIH under CO_2 atmosphere. Conditions: Photolysis carried out in a CO_2-saturated solution of DMF:TEOA (4:1 *v/v*) containing **Cu-PS** (0.5 mM), BIH (50 mM), xantphos (1 mM), T = 25 ºC, using Xe lamp irradiation (λ > 400 nm, 179 mW·cm^{-2}).

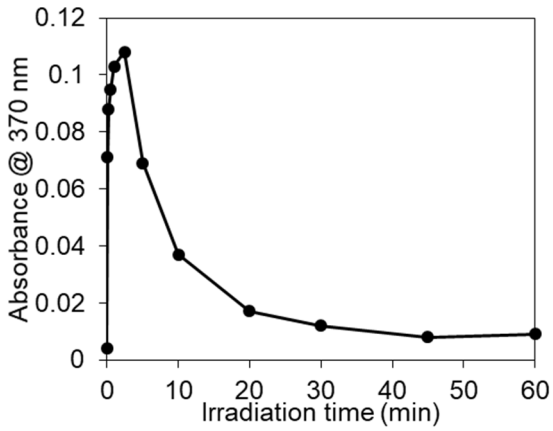

Fig. S44. Absorbance changes at 730 nm during photoirradiation. Conditions: Photolysis carried out in a CO_2-saturated solution of DMF:TEOA (4:1 *v/v*) containing **Cu-PS** (0.5 mM), BIH (50 mM), xantphos (1 mM), T = 25 ºC, using Xe lamp irradiation (λ > 400 nm, 179 mW·cm^{-2}).

12. Electrochemical experiments

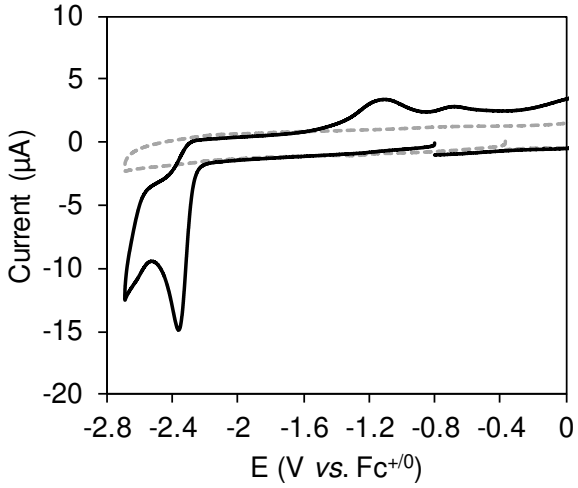

Fig. S45. CV of a 1 mM DMF solution of **4^{Zn}** at 100 mV·s^{-1} under Ar (GC working electrode, 0.1 M Bu_4NPF_6). The grey CV is the Ar saturated background. E(**LN4H$_2$**$^{0/\bullet-}$)= -2.36 V *vs.* Fc/Fc$^+$.

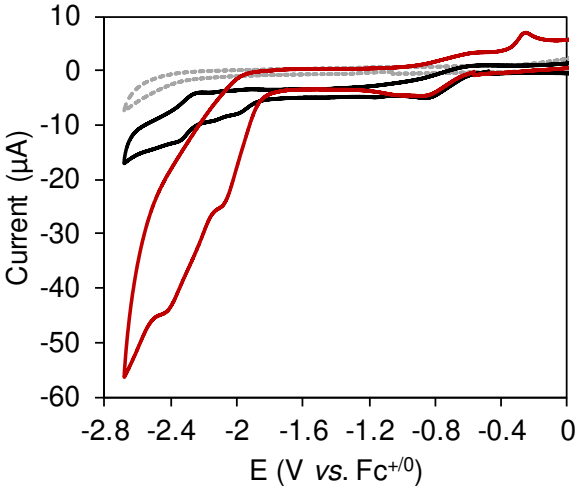

Fig. S46. CVs of a 1 mM DMF solution of **2^{Co}** at 100 mV·s^{-1} (GC working electrode, 0.1 M Bu_4NPF_6) under Ar (black) or CO_2 (red). The grey CV is the CO_2 saturated background. E($Co^{III/II}$)= -0.83 V, E($Co^{II/I}$)= -1.96 V, and E(**LN4H$_2$**$^{0/\bullet-}$)= -2.30 V *vs.* Fc/Fc$^+$.

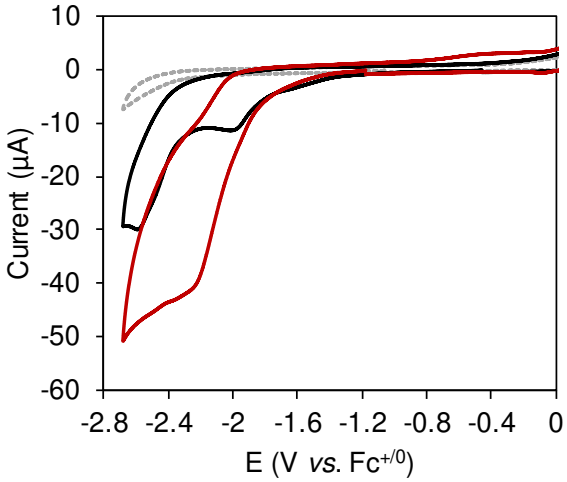

Fig. S47. CVs of a 1 mM DMF solution of $\mathbf{3^{Ni}}$ at 100 mV·s^{-1} (GC working electrode, 0.1 M Bu_4NPF_6) under Ar (black) or CO_2 (red). The grey CV is the CO_2 saturated background. E($Ni^{II/I}$)= -2.01 V, and E($\mathbf{LN4H_2}^{0/\bullet-}$)= -2.59 V *vs.* Fc/Fc$^+$.

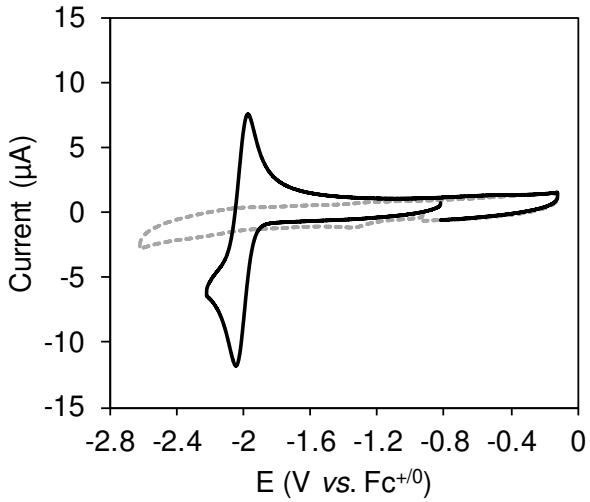

Fig. S48. CV of a 1 mM DMF solution of **Cu-PS** at 100 mV·s^{-1} under Ar (GC working electrode, 0.1 M Bu_4NPF_6). The grey CV is the CO_2 saturated background. $E_{1/2}$(**Cu-PS**/**Cu-PS**$^{\bullet-}$) = -2.01 V *vs.* Fc/Fc$^+$.

13. DFT Calculations

Density functional theory (DFT) calculations were performed using the Gaussian 09 software package.[26] The structures were fully optimized using the B3P86 density functional[27] with the effect of solvation in water taken into consideration using the conductor-like polarizable continuum model (C-PCM) method.[28] The B3P86/6-31+G(d,p) basis set was applied to all atoms. The use of B3P86/6-31+G(d,p) level of DFT was reported to show good consistency with theoretical and experimental results for first row transition metal complexes.[29]

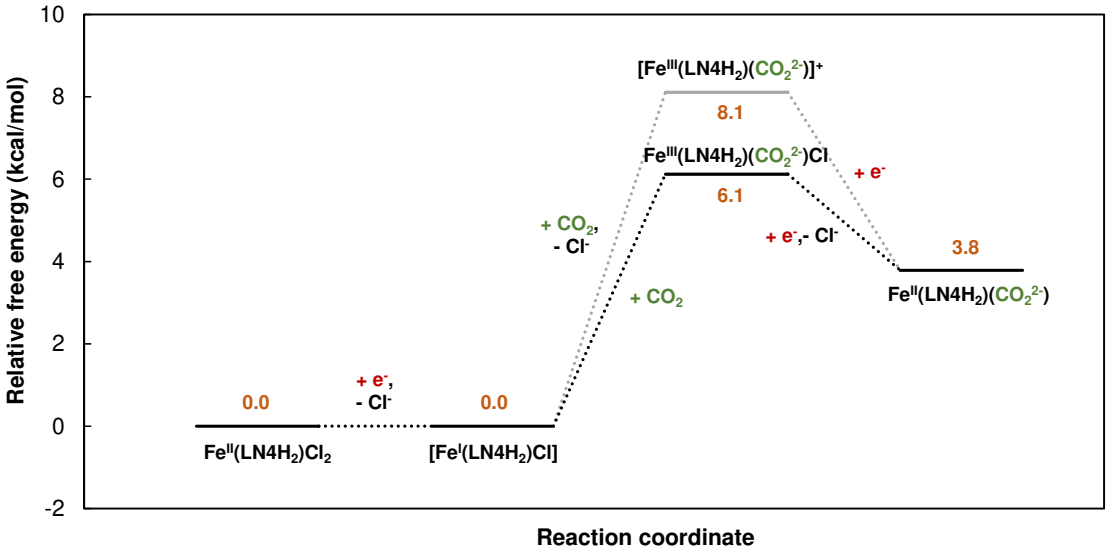

Fig. S49. Free energy diagram computed by DFT for the formation of CO_2-bound species in DMF, computed ay the B3P86/6-31+G(d,p) level.

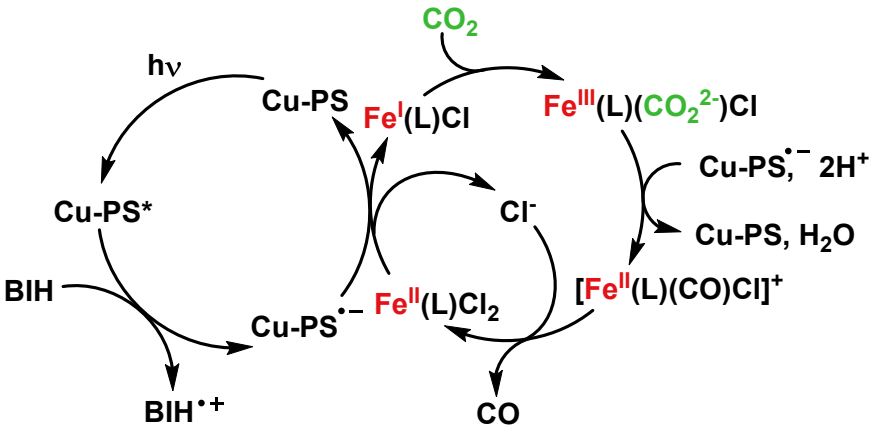

Scheme S6. Possible mechanism for the photocatalytic CO_2 reduction to CO in the **1**^{Fe}/**Cu-PS**/BIH/TEOA system. L denotes the **LN4H$_2$** ligand.

Table S13. DFT-optimized geometry of Fe^{II}(**LN4H$_2$**)Cl_2 (quartet), computed at the UB3P86/6-31+g(d,p) level using CPCM.

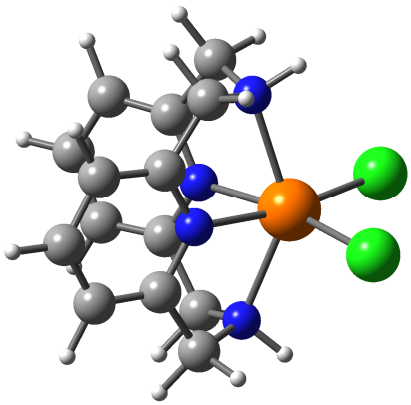

atom	x	y	z
C	-2.15055	-2.55793	-0.98937
C	-0.97469	-1.81249	-1.00695
C	-0.99885	-1.58701	1.308143
C	-2.17644	-2.32351	1.409371
C	-2.74827	-2.82205	0.241113
H	-2.59417	-2.90832	-1.91525
H	-2.63989	-2.48952	2.376005
H	-3.66938	-3.39416	0.28705
C	-2.17658	2.323424	-1.40934
C	-0.99899	1.586918	-1.30813
C	-0.97481	1.812415	1.006968
C	-2.15067	2.557858	0.989398
C	-2.7484	2.821961	-0.24108
H	-2.64004	2.489444	-2.37597
H	-2.59427	2.908255	1.91528
H	-3.66951	3.394076	-0.28701
N	-0.4194	-1.37011	0.124959
N	-0.41954	1.370026	-0.12495
N	0.50124	-0.19191	-2.14924
H	1.314987	-0.23418	-2.75421
N	0.501267	0.191901	2.149211
H	1.315045	0.234226	2.754131
C	-0.27672	1.006373	-2.50155
H	-0.99038	0.807782	-3.31089
C	-0.27658	-1.00645	2.501558
H	-0.99021	-0.80793	3.310947
C	-0.22554	-1.4661	-2.2714
H	0.520219	-2.24828	-2.44923
H	-0.91142	-1.46692	-3.12771
C	-0.22562	1.466043	2.2714
H	-0.91148	1.466787	3.127716

H	0.520084	2.248274	2.449231
H	0.427198	1.759241	-2.87293
H	0.427432	-1.75925	2.872884
Fe	1.271808	0.000038	-1.7E-05
Cl	2.867298	1.815018	0.058193
Cl	2.867402	-1.81482	-0.05821

SCF Done: E(UB3P86) = -2949.93552848 A.U. after 2 cycles
Annihilation of the first spin contaminant:
S**2 before annihilation 6.0086, after 6.0000

	1	2	3
	A	A	A
Frequencies --	41.8476	43.0983	50.2021
Red. masses --	5.1756	16.7738	8.5681

Zero-point correction= 0.292824 (Hartree/Particle)
Thermal correction to Energy= 0.312141
Thermal correction to Enthalpy= 0.313085
Thermal correction to Gibbs Free Energy= 0.242981
Sum of electronic and zero-point Energies= -2949.642704
Sum of electronic and thermal Energies= -2949.623387
Sum of electronic and thermal Enthalpies= -2949.622443
Sum of electronic and thermal Free Energies= -2949.692547

Item	Value	Threshold	Converged?
Maximum Force	0.000013	0.000450	YES
RMS Force	0.000004	0.000300	YES

Table S14. DFT-optimized geometry of $Fe^{I}(LN4H_2)Cl$ (quartet), computed at the UB3P86/6-31+g(d,p) level using CPCM.

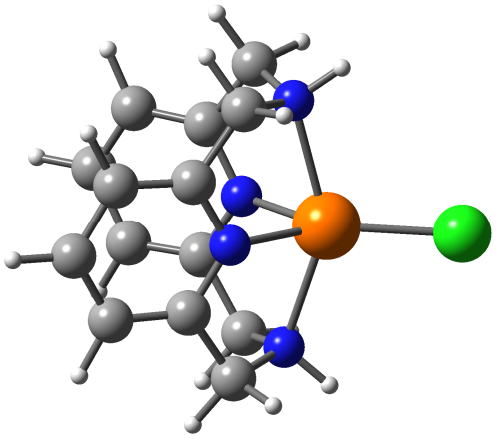

atom	x	y	z
C	2.025539	-1.20551	-2.12998
C	0.747839	-1.17076	-1.59266
C	0.748037	1.165694	-1.59618
C	2.025729	1.1986	-2.13362
C	2.677355	-0.00396	-2.42932
H	2.510023	-2.16217	-2.30074
H	2.510396	2.154649	-2.30729
H	3.677633	-0.00467	-2.84892
C	2.024699	-1.19871	2.134547
C	0.747383	-1.16572	1.5962
C	0.747332	1.170709	1.592678
C	2.024658	1.205393	2.130907
C	2.676172	0.003806	2.430705
H	2.509195	-2.15478	2.308554
H	2.509099	2.162021	2.301984
H	3.676143	0.004454	2.851037
N	0.096027	-0.00212	-1.36062
N	0.095626	0.002118	1.360215
N	-0.80432	-2.19963	0.00313
H	-1.60026	-2.82975	0.004079
N	-0.80421	2.199641	-0.00372
H	-1.60011	2.829826	-0.0049
C	-0.04137	-2.39811	1.248613

H	0.619898	-3.2734	1.199478
C	-0.04095	2.398049	-1.24907
H	0.620128	3.273476	-1.1999
C	-0.04139	-2.40188	-1.24181
H	-0.78089	-2.58987	-2.0301
H	0.619474	-3.27734	-1.19027
C	-0.04154	2.401937	1.241368
H	0.619546	3.277221	1.189825
H	-0.78115	2.590316	2.029478
H	-0.78076	-2.58434	2.037417
H	-0.78021	2.583955	-2.03808
Fe	-1.44471	0.000138	-0.00044
Cl	-3.74968	-3.4E-05	0.000137

SCF Done: E(UB3P86) = -2489.32992881 A.U. after 2 cycles
Annihilation of the first spin contaminant:
S**2 before annihilation 4.3709, after 3.7617

	1	2	3
	A	A	A
Frequencies --	25.1391	63.7550	72.6226
Red. masses --	14.2528	5.2078	3.5573

Zero-point correction= 0.289349 (Hartree/Particle)
Thermal correction to Energy= 0.306414
Thermal correction to Enthalpy= 0.307358
Thermal correction to Gibbs Free Energy= 0.243231
Sum of electronic and zero-point Energies= -2489.040580
Sum of electronic and thermal Energies= -2489.023515
Sum of electronic and thermal Enthalpies= -2489.022571
Sum of electronic and thermal Free Energies= -2489.086698

Item	Value	Threshold	Converged?
Maximum Force	0.000010	0.000450	YES
RMS Force	0.000002	0.000300	YES

Table S15. DFT-optimized geometry of $[Fe^{III}(LN4H_2)(CO_2^{2-})]^+$ (quartet), computed at the UB3P86/6-31+g(d,p) level using CPCM.

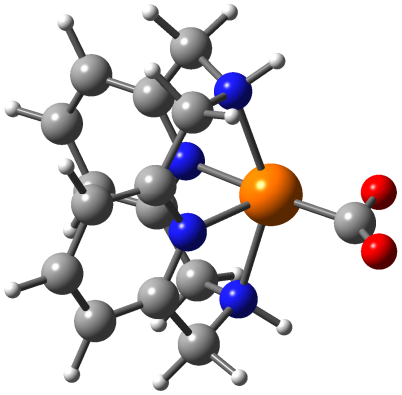

atom	x	y	z
C	3.278473	0.409497	-1.20591
C	1.919778	0.704721	-1.16738
C	1.919782	0.70476	1.167349
C	3.278478	0.409539	1.205884
C	3.962739	0.274869	-1.2E-05
H	3.783828	0.274814	-2.15592
H	3.783836	0.274889	2.155896
H	5.022155	0.040299	-0.00001
C	-0.42875	-3.02281	-1.20441
C	-0.65109	-1.65035	-1.16673
C	-0.65108	-1.65031	1.166788
C	-0.42875	-3.02277	1.204512
C	-0.33094	-3.71494	0.000061
H	-0.31749	-3.53188	-2.15549
H	-0.31748	-3.53181	2.155609
H	-0.15025	-4.78479	0.000079
N	1.28488	0.87295	-1.7E-05
N	-0.78586	-1.00681	0.000017
N	-0.35241	0.596479	-2.15547
H	-0.90308	1.202163	-2.75573
N	-0.3524	0.596549	2.155451
H	-0.90307	1.202254	2.755687
C	-0.77178	-0.7946	-2.40382
H	-0.2099	-1.24836	-3.22831
C	1.074029	0.882756	2.405634
H	1.473375	0.270401	3.222414
C	1.07402	0.882678	-2.40567
H	1.148349	1.928108	-2.72352
H	1.473363	0.270296	-3.22243
C	-0.77178	-0.79452	2.403851

H	-0.2099	-1.24826	3.228352
H	-1.82471	-0.7719	2.704943
H	-1.82472	-0.77199	-2.70491
H	1.148359	1.928197	2.723457
Fe	-0.79414	1.061398	-1.7E-05
C	-2.70681	1.377097	-0.00002
O	-3.8313	0.930291	-5.1E-05
O	-2.12901	2.508878	0.000018

SCF Done: E(UB3P86) = -2217.57546277 A.U. after 1 cycles
Annihilation of the first spin contaminant:
S**2 before annihilation 4.0157, after 3.7540

	106	107	108
	A	A	A
Frequencies --	3241.5890	3580.4101	3580.5840
Red. masses --	1.0987	1.0763	1.0763

Zero-point correction= 0.303844 (Hartree/Particle)
Thermal correction to Energy= 0.322237
Thermal correction to Enthalpy= 0.323182
Thermal correction to Gibbs Free Energy= 0.255942
Sum of electronic and zero-point Energies= -2217.271619
Sum of electronic and thermal Energies= -2217.253225
Sum of electronic and thermal Enthalpies= -2217.252281
Sum of electronic and thermal Free Energies= -2217.319521

Item	Value	Threshold	Converged?
Maximum Force	0.000017	0.000450	YES
RMS Force	0.000002	0.000300	YES

Table S16. DFT-optimized geometry of $Fe^{III}(LN4H_2)(CO_2^{2-})Cl$ (quartet), computed at the UB3P86/6-31+g(d,p) level using CPCM.

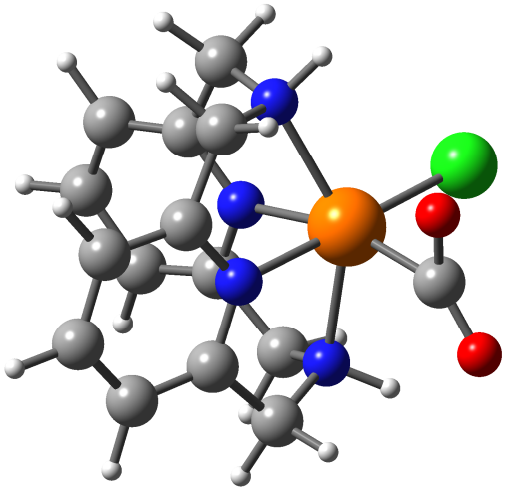

atom	x	y	z
C	2.84309	1.978962	-0.82467
C	1.540168	1.511128	-0.97558
C	1.212512	1.4842	1.326923
C	2.501717	1.953915	1.560155
C	3.320278	2.213957	0.462855
H	3.471401	2.142478	-1.69381
H	2.859542	2.097327	2.57413
H	4.333037	2.574344	0.611484
C	1.828918	-2.76398	-1.11686
C	0.806866	-1.82157	-1.18221
C	0.529059	-1.8656	1.12925
C	1.543353	-2.80687	1.274108
C	2.188177	-3.27143	0.129738
H	2.34247	-3.07647	-2.01978
H	1.830096	-3.15494	2.26069
H	2.98608	-4.00226	0.211989
N	0.753809	1.29813	0.084057
N	0.163671	-1.42149	-0.07852
N	-0.13487	0.197267	-2.24146
H	-0.84819	0.402614	-2.93353
N	-0.69931	0.091451	1.99763
H	-1.60676	0.225621	2.434411
C	0.335653	-1.18216	-2.46487

H	1.128018	-1.22563	-3.22173
C	0.22048	1.162105	2.417963
H	0.741499	0.91155	3.349553
C	0.904663	1.238502	-2.31863
H	0.419497	2.159803	-2.65908
H	1.676188	0.989265	-3.05727
C	-0.24887	-1.28181	2.283647
H	0.343383	-1.33104	3.204638
H	-1.14747	-1.88837	2.435465
H	-0.5154	-1.7553	-2.84648
H	-0.38393	2.054569	2.612857
Fe	-1.0978	0.254986	-0.1939
Cl	-2.42872	2.226591	-0.27996
C	-2.71971	-0.81634	0.072263
O	-2.81799	-1.03863	-1.14994
O	-3.33446	-1.10646	1.095046

SCF Done: E(UB3P86) = -2678.31294332 A.U. after 1 cycles
NFock= 1 Conv=0.37D-08 -V/T= 2.0062
Annihilation of the first spin contaminant:
S**2 before annihilation 4.0264, after 3.7579

	109	110	111
	A	A	A
Frequencies --	3237.6207	3572.4205	3583.1489
Red. masses --	1.0986	1.0763	1.0762

Zero-point correction= 0.303705 (Hartree/Particle)
Thermal correction to Energy= 0.324444
Thermal correction to Enthalpy= 0.325388
Thermal correction to Gibbs Free Energy= 0.252566
Sum of electronic and zero-point Energies= -2678.009238
Sum of electronic and thermal Energies= -2677.988499
Sum of electronic and thermal Enthalpies= -2677.987555
Sum of electronic and thermal Free Energies= -2678.060378

Item	Value	Threshold	Converged?
Maximum Force	0.000136	0.000450	YES
RMS Force	0.000018	0.000300	YES

Table S17. DFT-optimized geometry of $Fe^{II}(LN4H_2)(CO_2^{2-})$ (singlet), computed at the RB3P86/6-31+g(d,p) level using CPCM.

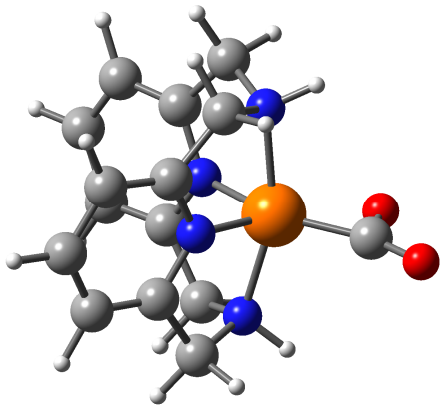

atom	x	y	z
C	3.133544	-0.78953	1.207861
C	1.746543	-0.86558	1.169731
C	1.747169	-0.86406	-1.16993
C	3.134196	-0.78793	-1.20721
C	3.833031	-0.75271	0.000535
H	3.655723	-0.75502	2.158156
H	3.656878	-0.75215	-2.15718
H	4.916171	-0.6899	0.000866
C	-0.08927	3.115115	1.20742
C	-0.45666	1.777315	1.172895
C	-0.45613	1.778511	-1.17155
C	-0.08871	3.116342	-1.20451
C	0.099339	3.794734	0.001843
H	0.04853	3.61611	2.15996
H	0.049577	3.618309	-2.15647
H	0.391706	4.839299	0.002439
N	1.086982	-0.9023	-0.00031
N	-0.62674	1.129545	0.000306
N	-0.53643	-0.51723	2.024795
H	-1.1885	-1.07391	2.570467
N	-0.53539	-0.51511	-2.02604
H	-1.18696	-1.07126	-2.57284
C	-0.78609	0.911397	2.353031
H	-0.25067	1.226039	3.255616

C	0.837918	-0.98024	-2.36192
H	1.243245	-0.4516	-3.23183
C	0.836557	-0.98317	2.36101
H	0.75936	-2.04229	2.630833
H	1.241434	-0.4558	3.231899
C	-0.78517	0.91384	-2.35271
H	-0.2496	1.229575	-3.25483
H	-1.85905	1.003818	-2.55329
H	-1.86	1.001307	2.553518
H	0.761209	-2.03901	-2.63323
Fe	-0.83311	-0.71683	-0.00049
C	-2.56506	-1.40885	-0.00085
O	-3.81272	-1.36945	-0.00082
O	-1.81657	-2.47821	-0.00123

SCF Done: E(RB3P86) = -2217.71816647 A.U. after 2 cycles

	106	107	108
	A	A	A
Frequencies --	3236.5095	3559.9695	3560.2015
Red. masses --	1.0982	1.0766	1.0767

Zero-point correction= 0.304370 (Hartree/Particle)
Thermal correction to Energy= 0.321651
Thermal correction to Enthalpy= 0.322595
Thermal correction to Gibbs Free Energy= 0.259916
Sum of electronic and zero-point Energies= -2217.413797
Sum of electronic and thermal Energies= -2217.396516
Sum of electronic and thermal Enthalpies= -2217.395571
Sum of electronic and thermal Free Energies= -2217.458250

Item	Value	Threshold	Converged?
Maximum Force	0.000027	0.000450	YES
RMS Force	0.000003	0.000300	YES

14. References

[1] S. P. Luo, E. Mejia, A. Friedrich, A. Pazidis, H. Junge, A. E. Surkus, R. Jackstell, S. Denurra, S. Gladiali, S. Lochbrunner, M. Beller, *Angew. Chem. Int. Ed.* **2013**, *52*, 419-423.

[2] Bruker, Bruker AXS Inc., Madison, Wisconsin, USA., **2013**.

[3] Bruker, Bruker AXS Inc., Madison, Wisconsin, USA., **2014**.

[4] O. V. Dolomanov, Bourhis, L. J., Gildea, R. J., Howard, J. A. K., Puschmann, H., *J. Appl. Cryst.* **2009**, *42*, 339-341.

[5] a) G. M. Sheldrick, *Acta Crystallogr., Sect. A: Found. Crystallogr.* **2008**, *64*, 112-122; b) G. M. Sheldrick, *Acta Crystallogr., Sect. A* **2015**, *71*, 3-8.

[6] L. J. Farrugia, *J. Appl. Crystallogr.* **1997**, *30*, 565.

[7] CCDC, **2001-2017**.

[8] POV-Ray, Persistence of Vision Pty. Ltd., Persistence of Vision Raytracer, retrieved from http://www.povray.org/download/, **2013**.

[9] A. L. Spek, *Acta Crystallogr., Sect. D: Biol. Crystallogr.* **2009**, *65*, 148-155.

[10] S. P. Westrip, *J. Appl. Crystallogr.* **2010**, *43*, 920-925.

[11] a) A. Rosas-Hernández, C. Steinlechner, H. Junge, M. Beller, *Green Chem.* **2017**, *19*, 2356-2360 ; b) H. Takeda, K. Ohashi, A. Sekine, O. Ishitani, *J. Am. Chem. Soc.* **2016**, *138*, 4354-4357; c) Z. Guo, S. Cheng, C. Cometto, E. Anxolabéhère-Mallart, S. M. Ng, C. C. Ko, G. Liu, L. Chen, M. Robert, T. C. Lau, *J. Am. Chem. Soc.* **2016**, *138*, 9413-9416; d) J.-X. Zhang, C.-Y. Hu, W. Wang, H. Wang, Z.-Y. Bian, *Appl. Catal. A* **2016**, *522*, 145-151; e) H. Rao, J. Bonin, M. Robert, *ChemSusChem* **2017**, *10*, 4447-4450; f) H. Rao, J. Bonin, M. Robert, *Chem. Commun.* **2017**, *53*, 2830-2833; g) H. Takeda, H. Kamiyama, K. Okamoto, M. Irimajiri, T. Mizutani, K. Koike, A. Sekine, O. Ishitani, *J. Am. Chem. Soc.* **2018**, *140*, 17241–17254; h) C. Steinlechner, A. F. Roesel, E. Oberem, A. Päpcke, N. Rockstroh, F. Gloaguen, S. Lochbrunner, R. Ludwig, A. Spannenberg, H. Junge, R. Francke, M. Beller, *ACS Catal.* **2019**, *9*, 2091-2100; i) L. Chen, Y. Qin, G. Chen, M. Li, L. Cai, Y. Qiu, H. Fan, M. Robert, T.-C. Lau, *Dalton Trans.* **2019**; j) C. Cometto, R. Kuriki, L. Chen, K. Maeda, T. C. Lau, O. Ishitani, M. Robert, *J. Am. Chem. Soc.* **2018**, *140*, 7437-7440; k) L. Lin, C. Hou, X. Zhang, Y. Wang, Y. Chen, T. He, *Appl. Catal., B* **2018**, *221*, 312-319; l) M. F. Kuehnel, C. D. Sahm, G. Neri, J. R. Lee, K. L. Orchard, A. J. Cowan, E. Reisner, *Chem. Sci.* **2018**, *9*, 2501-2509; m) M. F. Kuehnel, K. L. Orchard, K. E. Dalle, E. Reisner, *J. Am. Chem. Soc.* **2017**, *139*, 7217-7223; n) Q.-Q. Bi, J.-W. Wang, J.-X. Lv, J. Wang, W. Zhang, T.-B. Lu, *ACS Catal.* **2018**, *8*, 11815-11821.

[12] F. Bottino, M. Di Grazia, P. Finocchiaro, F. R. Fronczek, A. Mamo, S. Pappalardo, *J. Org. Chem.* **1988**, *53*, 3521-3529.

[13] F. Allen, *Acta Crystallogr., Sect. B: Struct. Sci.* **2002**, *58*, 380-388.

[14] A. L. Nivorozhkin, E. Anxolabéhère-Mallart, P. Mialane, R. Davydov, J. Guilhem, M. Cesario, J.-P. Audière, J.-J. Girerd, S. Styring, L. Schussler, J.-L. Seris, *Inorg. Chem.* **1997**, *36*, 846-853.

[15] N. Arulsamy, D. J. Hodgson, J. Glerup, *Inorg. Chim. Acta* **1993**, *209*, 61-69.

[16] T. Kojima, R. A. Leising, S. Yan, L. Que, *J. Am. Chem. Soc.* **1993**, *115*, 11328-11335.

[17] T. J. Hubin, J. M. McCormick, S. R. Collinson, N. W. Alcock, H. J. Clase, D. H. Busch, *Inorg. Chim. Acta* **2003**, *346*, 76-86.

[18] N. Raffard, R. Carina, A. J. Simaan, J. Sainton, E. Riviere, L. Tchertanov, S. Bourcier, G. Bouchoux, M. Delroisse, F. Banse, J.-J. Girerd, *Eur. J. Inorg. Chem.* **2001**, 2249-2254.

[19] H.-J. Krüger, *Chemische Berichte* **1995**, *128*, 531-539.

[20] T. W.-S. Chow, E. L.-M. Wong, Z. Guo, Y. Liu, J.-S. Huang, C.-M. Che, *J. Am. Chem. Soc.* **2010**, *132*, 13229-13239.

[21] S. P. Meneghetti, P. J. Lutz, J. Fischer, J. Kress, *Polyhedron* **2001**, *20*, 2705-2710.

[22] J. R. Khusnutdinova, J. Luo, N. P. Rath, L. M. Mirica, *Inorg. Chem.* **2013**, *52*, 3920-3932.
[23] K.F.W.Hekking, Q.Knijnenburg, T.M.Kooistra, P.H.M.Budzelaar, A.W.Gal, R.de Gelder, J.M.M.Smits, CSD Communication, **2003**.
[24] K. M. Lincoln, M. E. Offutt, T. D. Hayden, R. E. Saunders, K. N. Green, *Inorg. Chem.* **2014**, *53*, 1406-1416.
[25] R. Sanzenbacher, I. Sotofte, J. Springborg, *Acta Chem. Scand.* **1999**, *53*, 457-464.
[26] G. E. R. Scuseria, M. A.; Cheeseman, J. R.; Scalmani, G.; Barone, V.;, B. P. Mennucci, G. A.; Nakatsuji, H.; Caricato, M.; Li, X.; Hratchian,, A. F. B. H. P.; Izmaylov, J.; Zheng, G. ; Sonnenberg, J. L. ; Hada,, M. T. M.; Ehara, K.; Fukuda, R.; Hasegawa, J.; Ishida, M.; Nakajima,, Y. K. T.; Honda, O.; Nakai, H.; Vreven, T.; Montgomery, Jr., J. A.; Peralta,, F. B. J. E.; Ogliaro, M.; Heyd, J. J.; Brothers, E.; Kudin, K. N.;, V. N. K. Staroverov, R.; Normand, J.; Raghavachari, K.; Rendell,, J. C. I. A.; Burant, S. S.; Tomasi, J.; Cossi, M.; Rega, N.; Millam,, M. K. J. M.; Klene, J. E.; Cross, J. B.; Bakken, V.; Adamo, C.; Jaramillo,, R. S. J.; Gomperts, R. E.; Yazyev, O.; Austin, A. J.; Cammi, R.;, C. O. Pomelli, J. W.; Martin, R. L.; Morokuma, K.; Zakrzewski,, G. A. S. V. G.; Voth, P.; Dannenberg, J. J.; Dapprich, S.; Daniels,, F. A. D.; Farkas, J. B.; Ortiz, J. V.; Cioslowski, J.; Fox, D. J., I. Gaussian, Wallingford CT, **2009**.
[27] a) J. P. Perdew, *Phys. Rev. B* **1986**, *33*, 8822-8824; b) A. D. Becke, *J. Chem. Phys.* **1993**, *98*, 5648-5652.
[28] a) V. Barone, M. Cossi, *J. Phys. Chem. A* **1998**, *102*, 1995-2001; b) M. Cossi, N. Rega, G. Scalmani, V. Barone, *J. Comput. Chem.* **2003**, *24*, 669-681.
[29] a) B. H. Solis, Y. Yu, S. Hammes-Schiffer, *Inorg. Chem.* **2013**, *52*, 6994-6999; b) B. H. Solis, S. Hammes-Schiffer, *Inorg. Chem.* **2014**, *53*, 6427-6443.